Available on the CERN CDS information server

CMS PAS SMP-19-006
TOTEM NOTE 2020-001

CMS Physics Analysis Summary

Contact: cms-pag-conveners-smp@cern.ch

2020/04/17

Study of hard color singlet exchange in dijet events with proton-proton collisions at $\sqrt{s} = 13$ TeV

The CMS and TOTEM Collaborations

Abstract

This note presents a study of proton-proton collision events where the two leading jets are separated by a large pseudorapidity interval devoid of particle activity, known as jet-gap-jet events. Both jets have transverse momentum $p_{\mathrm{T,\,jet}} > 40$ GeV and pseudorapidity $1.4 < |\eta_{\text{jet}}| < 4.7$, with $\eta_{\text{jet-1}} \times \eta_{\text{jet-2}} < 0$. The analysis is based on data collected by the CMS experiment in proton-proton collisions during a low luminosity, high-β^* run in 2015 at $\sqrt{s} = 13$ TeV, with an integrated luminosity of 0.66 pb^{-1}. The number of charged particles detected with transverse momentum $p_{\mathrm{T}} > 200$ MeV in the fixed pseudorapidity interval $-1 < \eta < 1$ between the jets is used to discriminate jet-gap-jet events from color exchange dijet events. The fraction of jet-gap-jet events to all dijet events with similar kinematics, f_{CSE}, is presented as a function of the pseudorapidity difference between the leading two jets, the transverse momentum of the subleading jet, and the azimuthal angle separation between the leading two jets. The results are compared to previous measurements and to perturbative quantum chromodynamics predictions. In addition, the note presents the first study of jet-gap-jet events with a leading proton, interpreted as a proton-gap-jet-gap-jet topology, using a subsample of events collected by the CMS and TOTEM experiments with an integrated luminosity of 0.40 pb^{-1}. The leading protons are detected with the Roman pot detectors of the TOTEM experiment. The ratio f_{CSE} in this sample is found to be $2.91 \pm 0.70\ (\text{stat})^{+1.02}_{-0.94}\ (\text{syst})$ times larger than that for inclusive dijet production for dijets with similar kinematics.

1 Introduction

Quantum chromodynamics (QCD) is the established theory of strong interactions and is especially successful at very short distances, where physical observables can be computed in a perturbative expansion in powers of the strong coupling constant, α_s. However, there remain corners of phase space where predictions from perturbative QCD (pQCD) have yet to be confirmed. These regions, where the model comparisons are least complete, tend to be particularly important for understanding the initial state in hadronic collisions and for studies of high-energy scattering processes [1].

In scattering processes, the high-energy limit of QCD is mathematically represented by $\hat{s} \gg -\hat{t} \gg \Lambda^2_{\mathrm{QCD}}$, where $\hat{s}$ is the partonic center-of-mass energy squared, $\hat{t}$ is the partonic four-momentum transfer squared and Λ_{QCD} is the Landau pole of QCD. In this limit, large logarithms of $\hat{s}$ scale each power of α_s in the perturbative expansion, compensating for the smallness of $\alpha_s \approx 0.1$ such that $\alpha_s \ln\left(\frac{\hat{s}}{-\hat{t}}\right) \lesssim 1$. Here, the fixed-order perturbation theory approach is no longer valid. These logarithmically enhanced terms correspond to multiple parton splittings that are strongly ordered in rapidity. The Balitsky–Fadin–Kuraev–Lipatov (BFKL) evolution equation resums these terms to all orders in α_s in the perturbative expansion [2–4], and its solutions are known up to next-to-leading-logarithm (NLL) accuracy [5, 6]. In dijet production, the onset of BFKL dynamics can be reached in configurations where the two jets are separated by a large rapidity interval. The BFKL radiation pattern is also expected to emerge in the study of parton distribution functions (PDFs) of hadrons. In this context, the BFKL limit corresponds to the regime of very small values of the parton momentum fraction x_{Bj} at low virtualities Q^2. The resummation of $\ln(1/x_{\mathrm{Bj}})$ terms to all orders in α_s predicts a power-law growth of gluon densities at small x_{Bj}.

At the CERN LHC, dedicated studies of BFKL dynamics include measurements of azimuthal angle decorrelations between jets in forward-backward dijet configurations [7], and exclusive vector meson production with large four-momentum transfers [8–14]. Measurements of inclusive jet or multijet cross sections at various center-of-mass energies show no significant deviations from predictions based on the Dokshitzer–Gribov–Lipatov–Altarelli–Parisi (DGLAP) evolution equations [15–17], where parton emissions are strongly ordered in transverse momentum, distinct from the BFKL ordering in rapidity, over a large region of phase space [18–33]. State-of-the-art global PDF fits highlight the importance of including resummation of small x_{Bj} terms to all orders in α_s in order to describe inclusive deep inelastic scattering data collected by the HERA collider experiments [34]. A lesson from these studies is that BFKL dynamical effects associated with multiple parton splittings are very difficult to separate from other effects predicted by higher-order corrections in pQCD. More restrictive final-state studies, where other effects expected by pQCD are suppressed, may provide clearer hints of BFKL dynamics.

In this vein, a study of events in proton-proton (pp) collisions with two jets separated by a large pseudorapidity interval devoid of particle activity, known as Mueller-Tang jets [35] or jet-gap-jet events, is presented. Previous studies of jet-gap-jet events have been presented by the H1 and ZEUS Collaborations in dijet photoproduction in electron-proton collisions at the HERA collider [36, 37], by the CDF and D0 Collaborations in proton-antiproton ($\mathrm{p\bar{p}}$) collisions at $\sqrt{s} = 0.63$ and 1.8 TeV at the Tevatron [38–43], and by the CMS Collaboration at $\sqrt{s} = 7$ TeV in pp collisions at the LHC [44]. The pseudorapidity gap signature is indicative of an underlying t-channel hard color singlet exchange [45–48]. In the BFKL framework, the color singlet exchange is described by t-channel two-gluon ladder exchange between the interacting partons, as shown in Fig. 1, where the color charge carried by the exchanged gluons cancel, leading to suppression of particle production between the final-state jets. This is known as perturbative

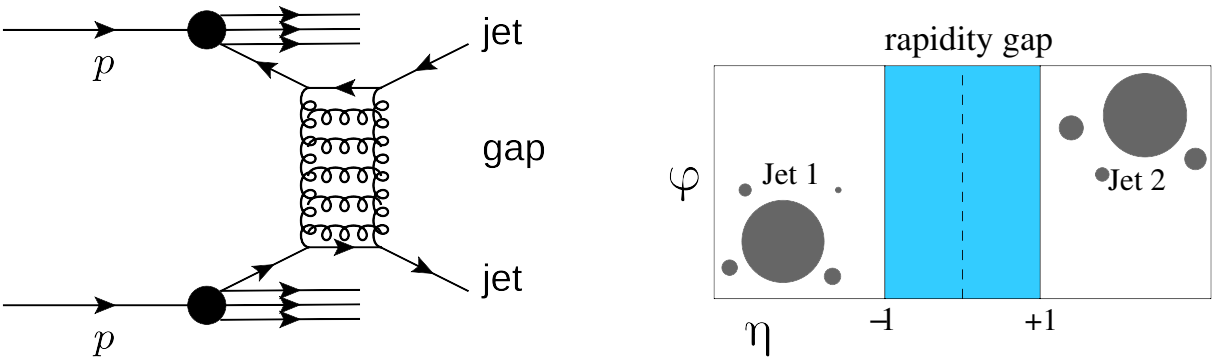

Figure 1: (Left) Schematic diagram of t-channel two-gluon exchange in pp collisions, which yields the jet-gap-jet signature reconstructed in the CMS detector. The lines adjacent to the protons represent the proton breakup. (Right) Jet-gap-jet event signature in the η–ϕ plane. The filled circles represent final-state particles. The filled area between the jets denotes the fixed pseudorapidity region $|\eta| < 1$ devoid of charged particle tracks.

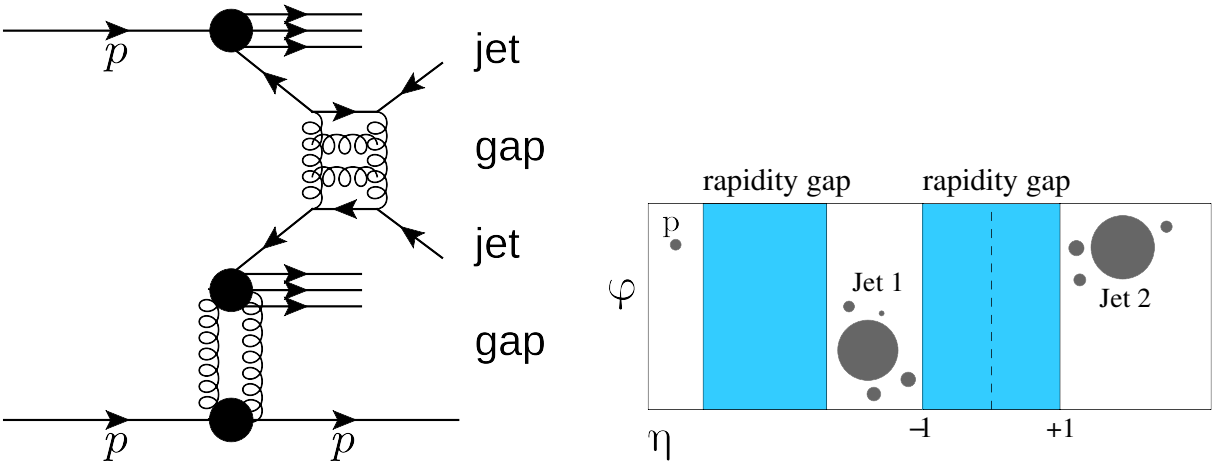

Figure 2: (Left) Schematic diagram of the production of jet-gap-jet event with a leading proton in pp collisions. The jet-gap-jet signature is observed in the CMS detector, while the leading proton is detected with the forward proton spectrometer of the TOTEM experiment. (Right) Proton-gap-jet-gap-jet event signature in the η–ϕ plane. The filled circles represent final-state particles. The filled areas denote the central gap region $|\eta| < 1$ where the charged particle track multiplicity is measured, and the forward rapidity gap which is inferred from the forward proton detection.

pomeron exchange. Color singlet exchange can occur in quark-quark, quark-gluon, and gluon-gluon scattering. The latter is expected to be largely favored due to the larger color charge of gluons [46–48]. On the other hand, in most collisions that lead to dijet production, the net color charge exchange between partons results in final-state particle production over wide intervals of rapidity between the jets. These color exchange dijet events are referred to in this note as "background" events. Dynamical effects predicted by DGLAP evolution equations are largely suppressed in events with pseudorapidity gaps, since the predicted dijet production rate is strongly reduced by way of a Sudakov form factor [45–48]. This form factor, which accounts for the probability of having no additional parton emissions between the hard partons, is not necessary for BFKL pomeron exchange [35]. The ratio of jet-gap-jet yields to inclusive dijet yields is highly sensitive to dynamical effects predicted by BFKL evolution equations [35].

The presence of soft rescattering effects between partons and the proton remnants modify the

visible cross section of jet-gap-jet events. These soft interactions can induce the production of particles in the interval of pseudorapidity that would otherwise be devoid of particles. This results in a reduction in the number of events identified as having a jet-gap-jet signature, with this reduction parametrized by means of a multiplicative factor known as the rapidity gap survival probability, $|\mathcal{S}|^2$. The survival probability is a process-dependent, nonperturbative quantity [45, 49–53] and, at LHC energies, is expected to have values of the order of $|\mathcal{S}|^2 = 1$–10%. This factor is believed to be largely independent of the dijet event kinematics, although some nonperturbative models, such as the soft color interactions model [54], suggest that this is not always the case. Multiparton interactions can contribute to the survival probability in dijet events with a central gap, as discussed in Ref. [55].

Soft rescattering effects can be suppressed by considering processes with color singlet exchange in the initial state of the hard scattering process, such as single- or central-diffractive dijet processes, or in dijet photoproduction, where the scattered proton(s) remain intact after the collision. These processes can be used to better separate events with a central gap between jets, as discussed in Ref. [56]. Thus, complementary to the study of jet-gap-jet events in inclusive dijet production, a study of jet-gap-jet events with a leading proton, as shown in Fig. 2, is also presented. Although no forward rapidity gap requirement is used in the analysis, these events are referred to as proton-gap-jet-gap-jet events throughout this note, where the forward rapidity gap signature is inferred from the leading proton detection. This part of the analysis uses a subsample of dijet events with leading protons detected with the forward proton spectrometers of the TOTEM experiment [57]. Such a diffractive event topology has not been previously studied.

The study presented in this note is based on low instantaneous luminosity data collected in pp collisions at $\sqrt{s} = 13$ TeV by the CMS and TOTEM detectors in 2015 at the CERN LHC. The 2015 run operated with special $\beta^* = 90$ m conditions, where β^* is the amplitude function at the interaction point [58]. The present study uses a similar event selection and central gap definition as in the previous measurement by CMS at 7 TeV [44]. Each of the leading two jets has transverse momentum $p_{\mathrm{T,\,jet}} > 40$ GeV and pseudorapidity $1.4 < |\eta_{\mathrm{jet}}| < 4.7$, with $\eta_{\text{jet-1}} \times \eta_{\text{jet-2}} < 0$. The charged particle multiplicity in the fixed pseudorapidity interval $|\eta| < 1$ between the leading two jets, where each charged particle has transverse momentum $p_{\mathrm{T}} > 200$ MeV, is used to separate the jet-gap-jet signal events from color exchange dijet events. Jet-gap-jet events appear as a sharp excess of events at the lowest multiplicities over the expected charged particle multiplicity distribution from color exchange dijet events, as determined using data-driven techniques. The increase in center-of-mass energy to 13 TeV and the large acceptance in pseudorapidity for jets reconstructed in CMS provide ideal conditions to study the color singlet exchange process in an unexplored region of phase space. The increased sample size relative to the previous analysis at 7 TeV allows for the use of finer binning in the kinematic variables of interest and for unprecedented precision in the determination of the ratio of jet-gap-jet yields to inclusive dijet yields. Furthermore, the second analysis, based on CMS and TOTEM data, allows for a first study of dijet events with a central gap and a leading proton. This latter study has the potential of further elucidating the role of soft parton exchanges in the creation and destruction mechanisms of pseudorapidity gaps in strong interactions. The leading protons considered in the analysis have a fractional momentum loss of up to 20%, with values of the square of the four-momentum transfer at the proton vertex in the range of $-4\ \mathrm{GeV}^2$ and $-0.025\ \mathrm{GeV}^2$.

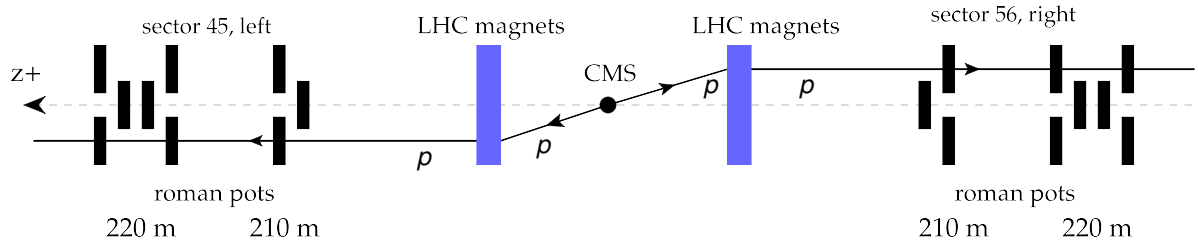

Figure 3: Side-view of detectors configuration during the 2015 CMS-TOTEM combined run. The horizontal dashed line indicates the beamline. The CMS detector is denoted by the filled circle in the center. The leading proton(s) are transported via the accelerator magnetic fields (blue rectangles), eventually passing through the silicon detectors housed in the Roman pots (black rectangles) of the TOTEM experiment. Sector 45 and sector 56 are located towards the positive and negative pseudorapidities in the CMS coordinate system, respectively.

2 The CMS and TOTEM detectors

The central feature of the CMS apparatus is a superconducting solenoid of 6 m internal diameter, providing a magnetic field of 3.8 T. Within the solenoid volume are a silicon pixel and strip tracker, a lead tungstate crystal electromagnetic calorimeter (ECAL), and a brass and scintillator hadron calorimeter (HCAL), each composed of a barrel and two endcap sections. Forward calorimeters extend the pseudorapidity coverage provided by the barrel and endcap detectors. Muons are detected in gas-ionization chambers embedded in the steel flux-return yoke outside the solenoid.

The silicon tracker measures charged particles within the pseudorapidity range $|\eta| < 2.5$. It consists of 1440 silicon pixel and 15 148 silicon strip detector modules. For nonisolated particles with $1 < p_{\mathrm{T}} < 10$ GeV and $|\eta| < 1.4$, the track resolutions are typically 1.5% in p_{T} and 25–90 (45–150) μm in the transverse (longitudinal) impact parameter [59].

Tracks are reconstructed with the standard iterative algorithm of CMS [59]. To reduce the misidentification rate, tracks are required to pass standard CMS quality criteria, referred to as high-purity criteria. High-purity tracks satisfy requirements on the number of hits and the χ^2 of the track-fit. The requirements are functions of the charged particle track transverse momentum p_{T} and pseudorapidity η, as well as the number of layers with a hit. A more detailed discussion on the combinatorial track-finding algorithm and the definition of high-purity tracks can be found in Ref. [59].

The particle-flow (PF) algorithm [60] aims to reconstruct and identify each individual particle in an event, with an optimized combination of information from the various elements of the CMS detector. The energy of photons is obtained from the ECAL measurement. The energy of electrons is determined from a combination of the electron momentum at the primary interaction vertex as determined by the tracker, the energy of the corresponding ECAL cluster, and the energy sum of all bremsstrahlung photons spatially compatible with originating from the electron track. The energy of muons is obtained from the curvature of the corresponding track. The energy of charged hadrons is determined from a combination of their momentum measured in the tracker and the matching ECAL and HCAL energy deposits, corrected for the response function of the calorimeters to hadronic showers. Finally, the energy of neutral hadrons is obtained from the corresponding corrected ECAL and HCAL energies.

The jets are clustered with the infrared and collinear-safe anti-k_{T} algorithm [61, 62], with a distance parameter of 0.4, starting from the particles reconstructed with the PF algorithm of CMS. The clustering is performed with the FastJet package [62]. The key feature of the anti-

k_T algorithm is the resilience of the jet boundary with respect to soft radiation. This leads to cone-shaped hard jets. The jet momentum is determined as the vector sum of all particle momenta in the jet, and is found in simulations of the CMS detector response to be within 5% and 10% of the true hadron-level momentum over a wide range of the jet transverse momentum and pseudorapidity values. Jet energy corrections are derived from the simulations to bring, on average, the measured jet energies to the known energies at the generator level. In situ measurements of the momentum balance in dijet, photon + jet, Z + jet, and multijet events are used to account for any residual differences in jet energy scale in data and simulation [63]. The jet energy resolution amounts typically to 15% at 10 GeV, 8% at 100 GeV, and 4% at 1 TeV. A more detailed description of the CMS detector, together with a definition of the coordinate system used and the relevant kinematic variables, can be found in Ref. [64].

The proton spectrometer of the TOTEM experiment consists of two sets of near-beam telescopes, known as Roman pot (RP) stations [57]. The arms are referred to as sector 45 and sector 56 for positive and negative pseudorapidities, respectively. A RP contains Si strip detectors that can approach the LHC beam at a distance of a few mm and can be used to detect protons deflected at scattering angles of only a few microradians relative to the beam without affecting the LHC operation [57]. During the 2015 special run, there were two RP stations operating in each sector located at ± 210 m and ± 220 m relative to the interaction point. The configuration during 2015 is depicted in Fig. 3. The station at 210 m has one unit of RPs, while the station at 220 m has two units of RPs. Each unit has three RPs: one located above ("top"), below ("bottom"), and to one side ("horizontal") of the LHC beam [57]. Before being detected, the trajectories of protons that have lost a small amount of their original momentum are slightly changed from the beam trajectory, with the deviation dependent on the momentum of the proton. The leading proton kinematics are reconstructed after modeling the transport of the protons from the interaction point to the RP location [57, 65]. With the $\beta^* = 90$ m conditions, small horizontal displacements of the forward proton tracks at the RPs are directly proportional to the proton fractional momentum loss, ξ. The detection of the forward protons enables also the reconstruction of the four-momentum transfer squared at the proton vertex, t, which is related to the horizontal and vertical scattering angles of the proton track at the RPs [66, 67]. The resolution in ξ is 0.8% for $\xi = 0$ and 0.2% for $\xi = 0.2$ [66]. The RPs are aligned following the standard techniques developed by the TOTEM Collaboration [66]. A full description of the TOTEM detector can be found in Refs. [57, 66].

3 Data sample and trigger selection

The pp collision data used in this analysis were collected in a combined special run by the CMS and TOTEM experiments in 2015, with the LHC operated at $\sqrt{s} = 13$ TeV in a mode with low probability of overlapping pp interactions in the same bunch crossing (pileup). With $\beta^* = 90$ m optics at the interaction point of CMS, there were about 0.05 – 0.10 interactions per bunch crossing. The CMS and TOTEM experiments collected data independently, and the samples were combined offline by matching bunch-crossing and orbit numbers. The integrated luminosity for the CMS dataset alone is 0.66 pb^{-1}, whereas for the combined CMS and TOTEM dataset it corresponds to 0.40 pb^{-1}. The data were collected with an unprescaled inclusive dijet trigger. This trigger required the presence of at least two jets with minimum transverse momentum of 32 GeV each, and with $|\eta| < 5$. The trigger is fully efficient when each of the leading jets has $p_T \geq 55$ GeV, as measured with dijet events in a zero-bias sample collected using a random trigger in the presence of non-empty bunch crossings. A subset of the zero-bias sample that contains forward proton information collected by the TOTEM experiment is used for systematic checks in the analysis. Trigger efficiency effects are suppressed in the ratio

of events with a central gap, the main observable measured in this study.

4 Event selection

4.1 Dijet event selection

The following selection requirements are used for the study of jet-gap-jet events within inclusive dijet events, as well as for the study of jet-gap-jet events with a leading proton:

- Each of the two leading jets are required to have transverse momentum of $p_{\mathrm{T,\,jet}} > 40$ GeV. This selection maximizes the number of dijet events considered in the analysis while ensuring high dijet reconstruction efficiency. The phase space explored in the present analysis is similar to that studied in the previous CMS measurement at 7 TeV [44]. There are no requirements on additional jets that may be produced in the collision.
- The two leading jets are measured in opposite hemispheres of the CMS detector, $\eta_{\text{jet-1}} \times \eta_{\text{jet-2}} < 0$, and have pseudorapidity values $1.4 < |\eta_{\text{jet-1, jet-2}}| < 4.7$. This selection favors the phase space region for production of jet-gap-jet events. Jets have a cone radius $R = 0.4$ and the adopted jet range thus locates the jets at least one cone radius away from the fixed pseudorapidity interval $|\eta| < 1$ used to extract the multiplicity of charged particles.
- The number of reconstructed primary vertices in the event is required to be at most one. This requirement is used to reject residual pileup interactions. A vertex with a minimum of two degrees of freedom is considered a primary vertex with this selection [59]. Keeping events with no primary vertex retains forward-backward dijet configurations that have too few tracks to establish a primary vertex, as is likely for the jet-gap-jet topology.
- The primary vertex, if present, is required to be located within a longitudinal distance of 24 cm of the nominal interaction point of CMS.

There are 362,915 dijet events satisfying these selection requirements.

4.2 Leading proton selection

For the study of jet-gap-jet events with a leading proton, in addition to the dijet event selection described in Section 4.1, the following selection requirements on the proton reconstructed in the RPs are also applied:

- At least one proton must be detected in either sector 45 or sector 56.
- The proton track has to cross at least two overlapping RP units (e.g., top-top, bottom-bottom), to ensure quality proton reconstruction.
- The fractional momentum loss of the proton ξ (hereafter referred to as $\xi_p(\mathrm{RP})$) has values of $\xi_p(\mathrm{RP}) < 0.2$, and the square of the four-momentum transfer at the proton vertex has values of $0.025 < -t < 4$ GeV^2. These bounds are based on acceptance studies of the RPs.
- The proton track impact points at the RPs satisfy the fiducial selection requirements of $8 < |y| < 30$ mm and $0 < x < 20$ mm for vertical RPs, and $|y| < 25$ mm and $7 < x < 25$ mm for horizontal RPs, where x and y denote the horizontal and vertical coordinates of the tracks in the transverse plane to the beamline at the RP, with the beam position centered in $x = y = 0$. This selection requirement ensures

good proton reconstruction efficiency and acceptance within the RPs, and is based on acceptance studies of the RPs.

Finally, in order to remove contributions of beam background events, which consist of dijet events paired with uncorrelated beam halo or pileup forward protons, the following additional condition is applied:

- Events satisfy $\xi_p(\mathrm{PF}) - \xi_p(\mathrm{RP}) < 0$, where $\xi_p(\mathrm{PF}) = \frac{\sum_i E^i \pm p_z^i}{\sqrt{s}}$ is the proton fractional momentum loss calculated with the PF candidates of the CMS detector. Here, E^i and p_z^i are the energy and longitudinal momentum of the i-th PF candidate in the event, respectively. The positive or negative sign in the sum corresponds to the scattered proton moving towards the positive or negative z direction in the CMS coordinate system, corresponding to the sector 45 or sector 56 directions, respectively. The PF candidates considered in the study have pseudorapidity values of $|\eta| < 5.2$ and energies above the noise level.

Ideally, it is expected that the fractional momentum loss reconstructed with the central detector or forward detectors should be the same, $\xi_p(\mathrm{PF}) = \xi_p(\mathrm{RP})$. However, because of reconstruction inefficiencies and acceptance limitations of the CMS detector, and the use of energy thresholds applied for each PF candidate reconstructed in CMS, these events satisfy instead the inequality $\xi_p(\mathrm{PF}) - \xi_p(\mathrm{RP}) < 0$, i.e. the fractional momentum loss is underestimated by the CMS detector. Therefore, the region $\xi_p(\mathrm{PF}) - \xi_p(\mathrm{RP}) > 0$ is dominated by events with uncorrelated forward protons which arise from pileup interactions or beam halo activity, since they do not have to satisfy the same bounds as the physical diffractive events. There is a residual contribution from these events in $\xi_p(\mathrm{PF}) - \xi_p(\mathrm{RP}) < 0$, which is subtracted from the data, as explained in Section 7.2. The selection requirement to suppress beam background contributions has also been used in the measurement of single-diffractive dijet production at $\sqrt{s} = 8$ TeV by the CMS and TOTEM Collaborations [68].

There are 336 and 341 events satisfying the dijet and leading proton selection requirements in sector 45 and sector 56, respectively.

5 Central gap between jets

Color singlet exchange dijet events cannot be identified on an event-by-event basis since color exchange dijet events may also have central pseudorapidity gaps through fluctuations in the particle activity between the two jets. However, the color singlet exchange dijet process is expected to lead to an increase in the number of dijet events at the lowest particle multiplicities over those arising from color exchange.

In this analysis, the charged particle multiplicity distribution between the two leading jets is used to define the pseudorapidity gap between jets. The multiplicity of charged particles, N_{Tracks}, is defined as the number of reconstructed charged particle tracks between the leading two jets, where each charged particle has transverse momentum $p_{\mathrm{T}} > 200$ MeV in the fixed pseudorapidity interval $|\eta| < 1$. The measured relative transverse momentum resolution of each charged particle is required to be smaller than 10%; this reduces the contribution from badly reconstructed or low-quality tracks. Reconstructed charged particle tracks satisfy the high-purity criteria of CMS [59]. The central gap corresponds to the absence of charged particle production in the pseudorapidity range $|\eta| < 1$. There are 1650 jet-gap-jet candidate events with $N_{\mathrm{Tracks}} = 0$ in the sample. While it is expected that jet-gap-jet events should only yield $N_{\mathrm{Tracks}} = 0$, events with multiplicities up to $N_{\mathrm{Tracks}} < 3$ are also considered in the analysis.

The latter consideration accounts for instances where jet constituents are emitted into the gap region, as discussed in Section 6.

The chosen pseudorapidity range of $|\eta| < 1$ ensures high reconstruction efficiency of charged particle tracks and, at the same time, is large enough to allow the subtraction of color exchange dijet contributions. The gap width used in the analysis is similar to that employed in previous measurements by the CDF, D0, and CMS Collaborations at lower $\sqrt{s}$. A larger fixed pseudorapidity interval results in a shift of the charged particle multiplicity distribution towards larger multiplicities. This mostly affects the color exchange dijet background, which is subtracted in the analysis, whereas the jet-gap-jet events remain mostly unaffected; jet-gap-jet events where the pseudorapidity range devoid of particle activity extends beyond the $|\eta| < 1$ limits are included with the nominal gap width choice.

For a central pseudorapidity gap definition with neutral hadrons or photons, the corresponding p_{T} thresholds cannot be lowered to the 200 MeV scale as with charged particle tracks. The noise level thresholds are 0.5 GeV and 2 GeV for photons and neutral particles at central pseudorapidities, respectively, which leads to a looser definition of a pseudorapidity interval devoid of particle activity. Consequently, neutral hadrons and photons are not used in the definition of the central pseudorapidity gap in this analysis.

When a leading proton is included, the same definition of the central gap between jets described above is used. The forward gap is inferred from the direct detection of the scattered proton, and no calorimeter-based rapidity gap is applied. A total of 11 events with $N_{\mathrm{Tracks}} = 0$ for dijet events with a leading proton is found.

Some features of the dijet sample enriched in jet-gap-jet events can be seen in Fig. 4. Events with $N_{\mathrm{Tracks}} = 0$ are dominated by jet-gap-jet events, while events with $N_{\mathrm{Tracks}} \geq 3$ are dominated by color exchange dijet events. Jet-gap-jet candidates have the two leading jets strongly correlated in their transverse momenta, as shown on the top panels of Fig. 4. This is characteristic of the nearly elastic parton-parton hard scattering process that initiated the jet production. The jet multiplicity, where each jet has transverse momentum of $p_{\mathrm{T,\,extra\text{-}jet}} > 15$ GeV and pseudorapidity $|\eta| < 4.7$, is shown on the bottom panel of Fig. 4. Most of the jet-gap-jet event candidates consist of two-jet events.

6 Observable

Ideally, jet-gap-jet signal events should only have $N_{\mathrm{Tracks}} = 0$. Occasionally, however, charged particles created during the fragmentation and hadronization processes are produced at large angles with respect to the initiated jet, such that they are emitted into the central pseudorapidity gap region. This leads to spillage of the jet-gap-jet signal events onto the neighboring multiplicity counts. Therefore, the jet-gap-jet contributions are extracted for multiplicities up to $N_{\mathrm{Tracks}} < 3$. This region is determined based on the background studies described in Section 7, which consistently yield an excess of events over the expected color exchange dijet event counts at low multiplicities.

The number of dijet events in the first bins of the multiplicity distribution $N_{\mathrm{Tracks}} < 3$ is denoted by N^{F}, the number of dijet events with no underlying color singlet exchange with $N_{\mathrm{Tracks}} < 3$ by $N^{F}_{\text{non-CSE}}$, and the number of dijet events with $N_{\mathrm{Tracks}} \geq 0$ by N. The yields N^{F} and N are extracted directly via event counting, whereas $N^{F}_{\text{non-CSE}}$ requires modeling of color exchange dijet events. The latter is treated with data-driven methods described in Section 7.

The fraction of color singlet exchange dijet events, f_{CSE}, is given by

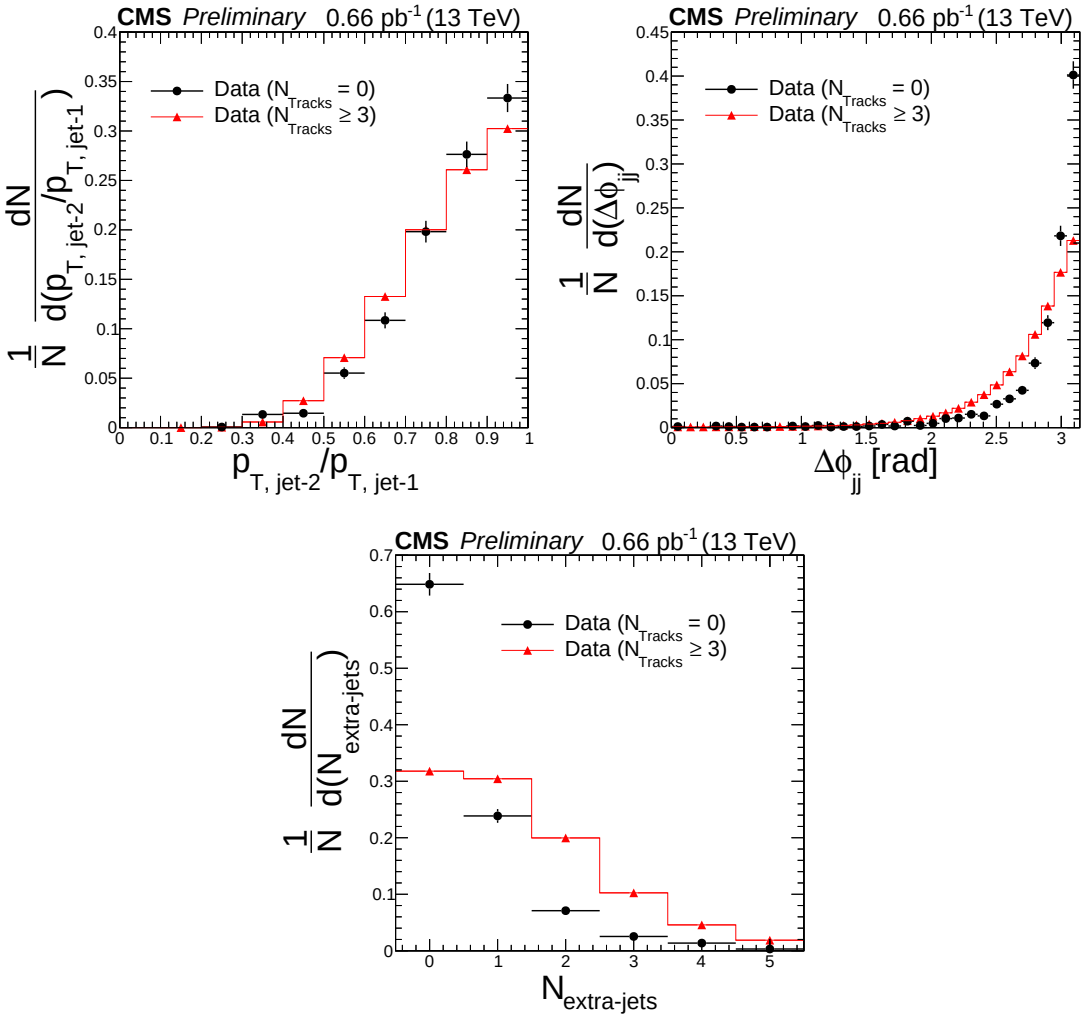

Figure 4: Distributions of the ratio of subleading jet transverse momentum to leading jet transverse momentum $p_{\mathrm{T,\,jet\text{-}2}}/p_{\mathrm{T,\,jet\text{-}1}}$ (left), azimuthal angle separation between leading two jets $\Delta\phi_{\mathrm{jj}}$(right), and number of additional jets $N_{\text{extra-jets}}$ with $p_{\mathrm{T,extra\text{-}jet}} > 15$ GeV (bottom), for jet-gap-jet candidates with $N_{\mathrm{Tracks}} = 0$ in $|\eta| < 1$ (black) and the color exchange dijet candidates $N_{\mathrm{Tracks}} \geq 3$ in $|\eta| < 1$ (red). The distributions are normalized to unity.

$$f_{\mathrm{CSE}} = \frac{N^{\mathrm{F}} - N^{F}_{\text{non-CSE}}}{N}, \tag{1}$$

and is measured as a function of kinematic variables of interest. As a ratio of yields, jet reconstruction uncertainties cancel in the f_{CSE} fraction. This fraction is determined as a function of:

- The pseudorapidity separation of the leading two jets, $\Delta\eta_{\mathrm{jj}} \equiv |\eta_{\text{jet-1}} - \eta_{\text{jet-2}}|$.
- The subleading jet transverse momentum, $p_{\mathrm{T,\,jet\text{-}2}}$.
- The azimuthal angle separation between the leading two jets, $\Delta\phi_{\mathrm{jj}} \equiv |\phi_{\text{jet-1}} - \phi_{\text{jet-2}}|$.

The fraction f_{CSE} as a function of $\Delta\eta_{\mathrm{jj}}$ is particularly sensitive to predictions based on perturbative calculations within the BFKL framework [54, 69–71] since it is directly related to the resummation of large logarithms of energy. The fraction as a function of $p_{\mathrm{T,\,jet\text{-}2}}$ addresses phenomenology studies that predict a weak dependence of this fraction on $p_{\mathrm{T,\,jet\text{-}2}}$ based on BFKL calculations [54, 69–71]. This $p_{\mathrm{T,\,jet\text{-}2}}$ dependence also allows for a better comparison with previous measurements by the D0 [39, 40] and CMS [44] Collaborations. The jet-gap-jet fraction as a function of $\Delta\phi_{\mathrm{jj}}$ is sensitive to deviations from the back-to-back topology of jet-gap-jet events caused by higher-order perturbative corrections, e.g. those caused by corrections to the coupling of the perturbative pomeron exchange to the proton PDFs embedded in the so-called impact factors. The jet-gap-jet fraction is extracted in bins of the kinematic variables of interest with ranges specified in Tables 2, 3, 4 of Section 9.1.

For the study with leading protons, the gap fraction is calculated such that it quantifies the ratio of the number of proton-gap-jet-gap-jet events to the number of proton-gap-jet-jet events. In this case, the signal region is integrated in the first two multiplicity bins, $N_{\mathrm{Tracks}} < 2$, because of the lower mean multiplicity in the proton tagged sample found in data, as shown in Section 7.2. Because of the limited sample size, a measurement as a function of kinematic variables is not possible. Thus, the gap ratio is extracted within the whole sample of events with leading protons.

7 Background treatment

Two independent, data-driven techniques are used to describe the contribution of color exchange dijet events in the lowest multiplicity bins. The first method relies on a data sample orthogonal to the nominal sample, while the second method relies on a parametrization of particle multiplicity distributions in hadronic collisions. These techniques avoid model-dependent treatment of the underlying event activity, hadronization effects, and other effects that impact the description of particle activity between the jets in Monte Carlo event generators.

7.1 Background for jet-gap-jet events

In the first approach, a separate charged particle multiplicity distribution is obtained from a sample of events where the two leading jets are reconstructed on equal sides of the CMS detector ($\eta_{\text{jet-1}} \times \eta_{\text{jet-2}} > 0$) with jets satisfying the requirements $1.4 < |\eta_{\text{jet-1, jet-2}}| < 4.7$ and $p_{\mathrm{T,\,jet\text{-}2}} > 40$ GeV. This orthogonal sample of dijet events is referred hereafter as "ES dijet sample," with the nominal sample ($\eta_{\text{jet-1}} \times \eta_{\text{jet-2}} < 0$) denoted by "OS dijet sample." In order to suppress single-diffractive dijet contributions (gap-jet-jet topology) in the ES sample, which can affect the shape of the multiplicity distribution at very low multiplicities, at least one calorimeter tower in the forward region opposite to the dijet system within $3 < |\eta| < 5$ is required,

with a minimum energy deposition of 5 GeV above calorimeter noise level.

The multiplicity distribution of charged particles in $|\eta| < 1$ is biased differently in the ES sample relative to the OS sample. To compensate for this bias and obtain a better superposition of the charged particle multiplicity distributions of the ES dijet sample and the OS dijet sample for multiplicities of $N_{\text{Tracks}} \geq 3$, the fixed pseudorapidity interval for the ES dijet sample is adjusted. The adjustment is found by matching the mean multiplicity of the distributions of the ES and OS samples by varying the pseudorapidity gap width in the ES sample. The optimal gap region for the ES dijet sample is $|\eta| < 1.2$, consistent with findings by the CDF and CMS Collaborations [41–44]. The multiplicity distribution in the ES sample is normalized to the one of the OS dijet sample in the control region $3 \leq N_{\text{Tracks}} \leq 40$. The number of events of the ES sample in the first multiplicity bins $N_{\text{Tracks}} < 3$ is then taken as the number of color exchange events, as illustrated in Fig. 5 for one of the bins in $p_{\text{T,jet-2}}$ used in the analysis. An excess of OS dijet events at low multiplicities above the expected color exchange counts is observed.

The second method used to estimate the color exchange background relies on a fit to the charged particle multiplicity distribution with a negative binomial distribution (NBD) function. This distribution can be used to describe charged particle multiplicity distributions with underlying color charge exchanges in hadronic collisions [72, 73], as first noted by the UA5 Collaboration [74, 75] at $\sqrt{s} = 540$ GeV. The NBD functional form has also been used to describe pp collision data at several $\sqrt{s}$ by the ALICE Collaboration [76]. It has been noted that the NBD function is less successful in describing the high multiplicity tails of particle multiplicity distributions for center-of-mass energies larger than 900 GeV [75, 76], making the use of more complex phenomenological parametrizations necessary for very wide multiplicity intervals. For the study of jet-gap-jet events considered in this note, a single NBD function fit is sufficient, since the main focus is at low multiplicities.

The NBD function is fit in the interval $3 \leq N_{\text{Tracks}} \leq 35$, which is dominated by color exchange dijet events, and is extrapolated down to $N_{\text{Tracks}} = 0$ to estimate the contribution of color exchange dijet background counts, as illustrated in Fig. 5 for one of the bins in $p_{\text{T,jet-2}}$ used in the analysis. The estimated color exchange dijet yield in the signal region is stable with respect to variations of the starting and ending points of the fit region, as verified by varying the fit range, with studies done with $3 \leq N_{\text{Tracks}} \leq 25$, $3 \leq N_{\text{Tracks}} \leq 45$, and $4 \leq N_{\text{Tracks}} \leq 35$. The NBD method for estimating the color exchange contributions in jet-gap-jet analyses has been used by the D0 and CMS Collaborations [38–40, 44].

The NBD method is used to extract the main results in the analysis, since it allows for the computation of the fraction f_{CSE} as a function of the kinematic variables of interest. The ES method is used for systematic checks in the analysis. The ES method overestimates the contribution of color exchange events by around 15% relative to the results extracted with the NBD method in $40 < p_{\text{T, jet-2}} < 50$ GeV, and values of 1–5% for larger values of transverse momentum $p_{\text{T, jet-2}} > 50$ GeV. These differences are assigned as a systematic uncertainty.

The performance of the NBD method is tested on the multiplicity distribution of charged particles of the ES dijet sample by performing the NBD fit in the range $3 \leq N_{\text{Tracks}} \leq 35$. The extrapolation of the fit results down to $N_{\text{Tracks}} = 0$ agrees with the ES data. As an additional check, a subset of the OS dijet sample characterized by the presence of a third central jet with transverse momentum $p_{\text{T, jet-3}} > 15$ GeV and pseudorapidity $|\eta_{\text{jet-3}}| < 1$ is studied. This selection yields a trijet sample enriched in color exchange events. The NBD function fit describes correctly the charged particle multiplicity distribution of this trijet sample, further confirming the validity of the NBD approach.

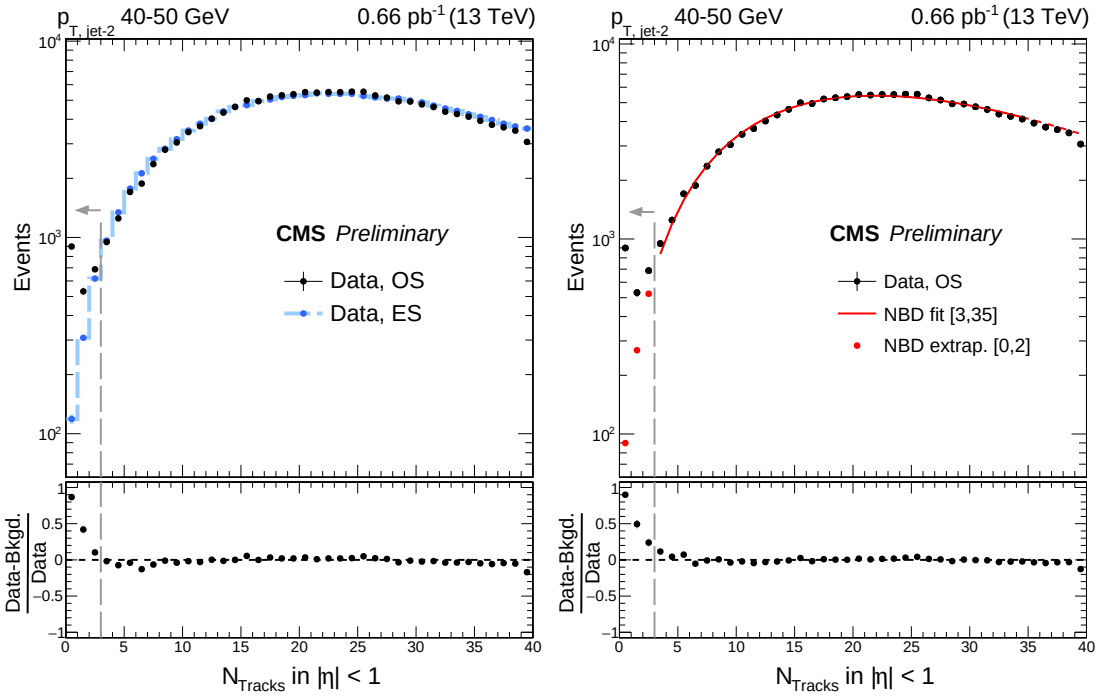

Figure 5: Charged particle multiplicity distribution in the fixed pseudorapidity region $|\eta| < 1$ for charged particle tracks with $p_{\mathrm{T}} > 200$ MeV for dijet events with $40 < p_{\mathrm{T,\,jet\text{-}2}} < 50$ GeV. Opposite side (OS) dijet events satisfy $\eta_{\mathrm{jet\text{-}1}} \times \eta_{\mathrm{jet\text{-}2}} < 0$. Vertical bars, which represent statistical uncertainties, are smaller than the markers for most data points. Results from color exchange dijet background estimation based on the equal side (ES) dijet events and the negative binomial distribution (NBD) function fit are shown on the left and right panels, respectively. The NBD function is fit in $3 \leq N_{\mathrm{Tracks}} \leq 35$, and extrapolated down to $N_{\mathrm{Tracks}} = 0$. The vertical dashed line represents the jet-gap-jet signal region used in the analysis, $N_{\mathrm{Tracks}} < 3$. The fraction f_{CSE} corresponds to the ratio of the excess of events at low multiplicities relative to the integrated number of events, as described in text. The dashed curve in $N_{\mathrm{Tracks}} > 35$ on the right panel is an extrapolation of the NBD fit.

The f_{CSE} fractions are extracted from the data using dijet yields uncorrected for detector effects. No unfolding of the data is necessary, since reconstruction, resolution and migration effects cancel in the ratio of yields in f_{CSE}. The number of color singlet exchange dijet events is not affected by track reconstruction inefficiencies; the latter only influences the color exchange dijet event counts, which are subtracted in the analysis. Studies with simulated events show that the results do not change within uncertainties if generator-level variables are used. Stable particles, whose decay length is greater than 20 mm, are used for jet reconstruction and measurement of charged particle multiplicity distribution between the jets, and compared to the results after considering the detector response. For these simulation studies, inclusive dijet events (with no hard color singlet exchange contributions) were simulated using the leading order (LO) PYTHIA8 Monte Carlo event generator [77] (version 8.212) with the PDF set NNPDF2.3LO [78, 79]. PYTHIA8 relies on parton showering algorithm for resummation of soft and collinear gluon emissions at leading-logarithm accuracy, and on the Lund string fragmentation model for hadronization effects [80]. The underlying event tune CUETP8M1 is used [81], together with initial- and final-state radiation effects. Hard color singlet exchange events are simulated with the HERWIG6 Monte Carlo event generator [82] (version 6.520) with the PDF set CTEQ6L1 [83]. The HERWIG6 generator simulates events with hard color singlet exchange between two partons following predictions based on simplified leading-logarithm BFKL calculations. Hadronization effects in HERWIG are based on the cluster fragmentation model [84]. Multiparton interactions are supplemented by the JIMMY package [85]. A detailed simulation of the CMS detector response is performed with the GEANT4 toolkit [86]. The f_{CSE} ratios calculated with PYTHIA8 predictions are consistent with the values extracted using the data-driven techniques, within uncertainties.

7.2 Background for proton-gap-jet-gap-jet events

In considering the sample with leading protons, the contribution of protons from pileup interactions and beam halo activity has to be subtracted. The residual contamination that survives the selection requirement $\xi_p(\mathrm{PF}) - \xi_p(\mathrm{RP}) < 0$ described in Section 4.2 is estimated using an event mixing procedure that mimics the beam background contribution in the nominal sample, as described below.

Events from the inclusive dijet sample are paired with uncorrelated protons from events in the zero-bias data sample. The number of events from this event mixing procedure is normalized to data with $\xi_p(\mathrm{PF}) - \xi_p(\mathrm{RP}) > 0$, which is dominated by beam background events. Then, the number of events with $\xi_p(\mathrm{PF}) - \xi_p(\mathrm{RP}) < 0$ is taken as the estimated number of beam background events present in the nominal sample. The results of this procedure can be seen in Fig. 6. Beam background contamination constitutes 13.4% and 15.5% of the sample in sector 45 and sector 56, respectively. Similar procedures have been used in Refs. [68, 87–92].

Standard single-diffractive dijet events (proton-gap-jet-jet topology) can feature a proton-gap-jet-gap-jet signature by fluctuations in the charged particle multiplicity between the jets. The methods introduced in Section 7.1 are used to estimate these contributions with modifications that account for differences in the sample with leading protons.

The first approach is the ES method. For this analysis, the definition of the orthogonal dijet sample introduced in Section 7.1 cannot be used for dijet events with leading protons. This is because single-diffractive dijet events are intrinsically boosted along the beam direction, in a direction opposite to the scattered proton. This usually leads to a final-state gap-jet-jet topology, where the mean pseudorapidity of the jets is not centered at 0. Thus, in considering single-diffractive dijet events located in the same hemisphere of the CMS detector, the multiplicity of

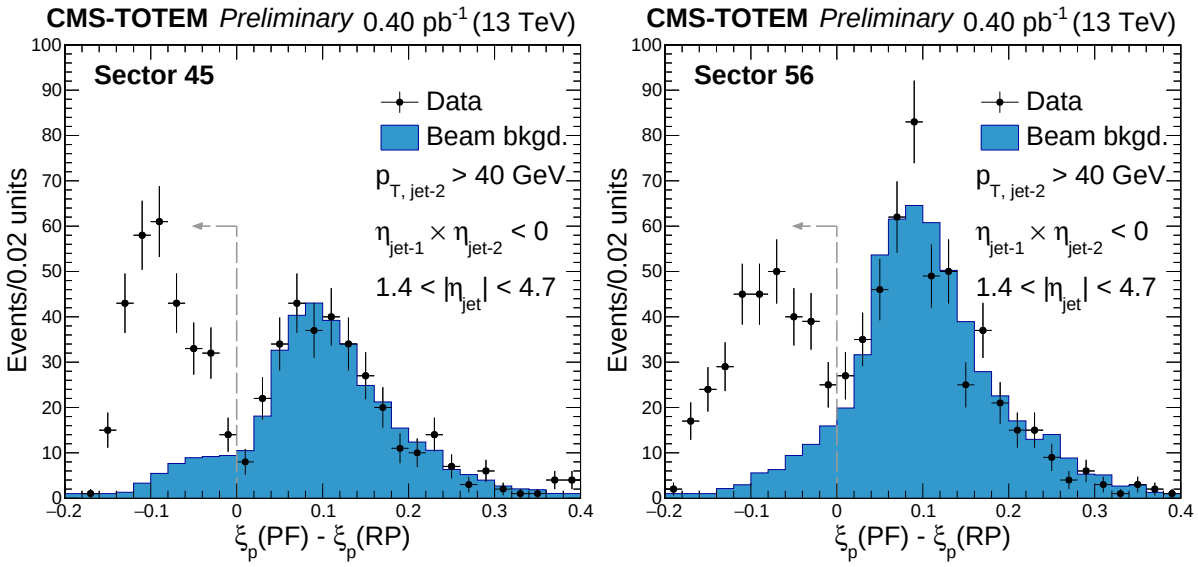

Figure 6: Distribution of $\xi_p(\mathrm{PF}) - \xi_p(\mathrm{RP})$ in sector 45 (left) and sector 56 (right) in data, where $\xi_p(\mathrm{PF})$ and $\xi_p(\mathrm{RP})$ denote the fractional momentum loss of the proton reconstructed with the particle-flow (PF) candidates of CMS and the Roman pots (RP) of TOTEM, respectively. Vertical bars indicate statistical uncertainties only. The estimated background contamination (beam background events) is represented by the filled histogram, and is estimated from the data, as described in text. No central pseudorapidity gap is required for this plot. The vertical dashed line represents the requirement applied in the analysis to remove most of the beam background contribution.

charged particles in $|\eta| < 1.2$ is directly influenced by the aforementioned effect. To account for this effect, the charged particle multiplicity distribution of the orthogonal dijet sample is instead measured in shifted intervals of pseudorapidity $-2 < \eta < 0.4$ and $-0.4 < \eta < 2$ for protons detected in sector 45 and sector 56, respectively. These intervals are determined based on the mean jet pseudorapidity found in data for events with a leading proton in sector 45 and sector 56, which corresponds to boosts of about 0.8 units in negative pseudorapidities and positive pseudorapidities, respectively. The leading two jets are located on the same side relative to these fixed pseudorapidity intervals. Each jet axis is at least 0.2 units of pseudorapidity away from the edges of the pseudorapidity region. The resulting distribution is normalized in the range $3 \leq N_{\mathrm{Tracks}} \leq 40$ to the multiplicity distribution of charged particles of the nominal sample, and the number of events of the ES sample in the lowest multiplicity bins is then used to estimate the proton-gap-jet-jet contribution in that region, as shown in Fig. 7. An excess of events over the expected background counts is observed, which is attributed to the presence of proton-gap-jet-gap-jet events.

The second approach is based on the NBD method introduced in Section 7.1. The NBD function is fit in the interval $2 \leq N_{\mathrm{Tracks}} \leq 25$, and extrapolate the fit to $N_{\mathrm{Tracks}} = 0$ to estimate the contribution of proton-gap-jet-jet events which feature a central gap, as seen in Fig. 7. An excess over the NBD extrapolation results is observed, which can be explained by the presence of proton-gap-jet-gap-jet events. The upper bound at $N_{\mathrm{Tracks}} = 25$ is chosen to take into account the lower mean multiplicity of the sample with leading protons, and to avoid contributions by beam background contamination that dominate at high multiplicities $N_{\mathrm{Tracks}} \geq 35$. The NBD method is used to extract the main results in the analysis.

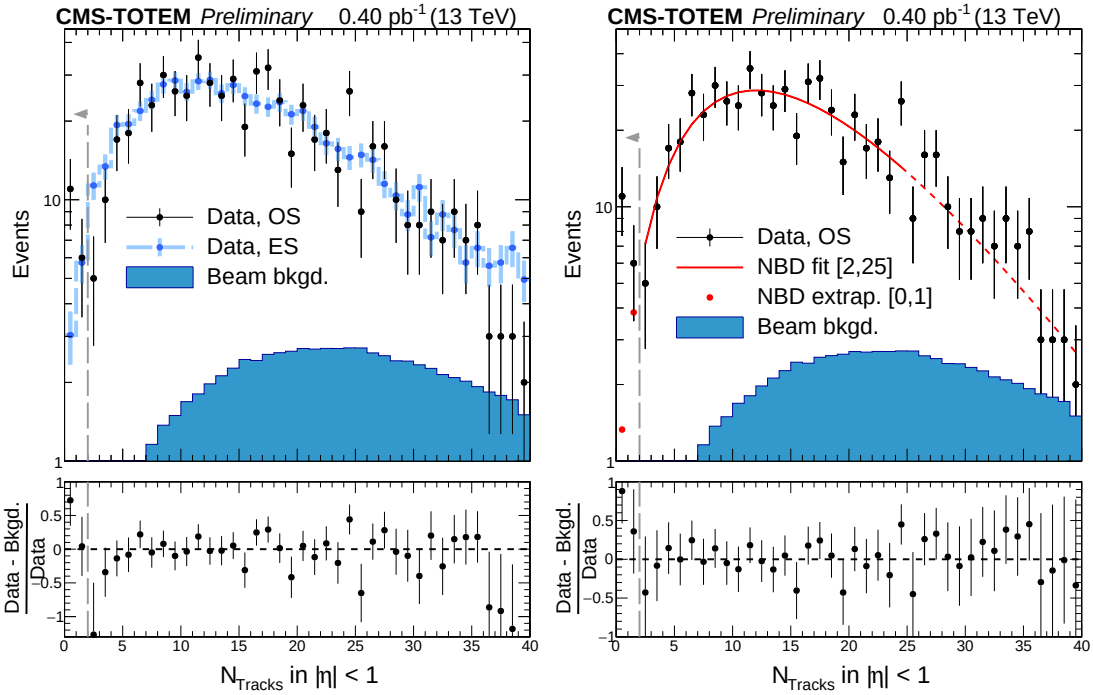

Figure 7: Charged particle multiplicity distribution in the fixed pseudorapidity region $|\eta| < 1$ after the dijet selection and proton selection. Opposite side (OS) dijet events satisfy $\eta_{\text{jet-1}} \times \eta_{\text{jet-2}} < 0$. Vertical bars indicate statistical uncertainties. The filled histogram represents the residual beam related contamination. The contribution of proton-gap-jet-jet events which feature a central gap is modeled with the equal side (ES) dijet events (left) and with the negative binomial distribution (NBD) function fit (right), as described in text. The NBD function is fit in $2 \leq N_{\text{Tracks}} \leq 25$, and extrapolated down to $N_{\text{Tracks}} = 0$. The vertical dashed line represents the jet-gap-jet signal region used in the analysis, $N_{\text{Tracks}} < 2$. An excess is observed in the lowest charged particle multiplicity bins, which corresponds to the presence of proton-gap-jet-gap-jet events in the sample. The dashed curve on the right panel represents an extrapolation of the NBD fit to $N_{\text{Tracks}} > 25$.

8 Systematic uncertainties

8.1 Systematic uncertainties in study of jet-gap-jet events

The sources of systematic uncertainties considered for the gap fraction f_{CSE} measurement are:

- **Jet energy scale:** The transverse momentum p_{T} of each jet is varied with $p_{\mathrm{T}} \to p_{\mathrm{T}} \pm \delta p_{\mathrm{T}}(p_{\mathrm{T}}, \eta)$, where $\delta p_{\mathrm{T}}(p_{\mathrm{T}}, \eta)$ is the jet energy scale uncertainty as a function of the jet p_{T} and η. The new jet collection is reordered in transverse momentum, and the analysis is repeated. The difference in the extracted gap fraction f_{CSE} relative to the results found with the nominal jet energy corrections is taken as a measure of the associated systematic uncertainty. The relative uncertainty has a size of 0.5–6%.
- **Track quality criteria:** The selection criteria used to define high-purity tracks are loosened and the difference in the gap fraction with respect to the nominal selection is taken as a systematic uncertainty. The loose quality criteria considers the minimum requirements for a track to be kept in the general track collection of CMS [59]. The track quality uncertainty is found to be 1.5–8%.
- **Charged particle transverse momentum p_{T} threshold:** Charged particles with transverse momentum below 200 MeV are not considered in identifying a central pseudorapidity gap. To study the sensitivity of the results to this threshold, the analysis is repeated with p_{T} thresholds of 150 MeV and 250 MeV. The corresponding relative differences in the measured gap fractions are 1–6% and are included as systematic uncertainties.
- **Background subtraction method**: The background determined using the ES method is compared to the adopted NBD background approach, with the difference taken as the associated systematic uncertainty. This reflects the imperfect knowledge of charged particle multiplicity distributions of color exchange dijet events. At low transverse momentum $40 < p_{\mathrm{T,\,jet\text{-}2}} < 50$ GeV the relative systematic uncertainty is 14.6%, while for larger transverse momentum $p_{\mathrm{T,\,jet\text{-}2}} > 80$ GeV it is 2–5%.
- **NBD fit parameters uncertainties:** The NBD function considered in the analysis has three free parameters, including an overall normalization. The color exchange dijet yields in the signal region are estimated by varying the NBD fit parameters within their uncertainties. Correlations between the fit parameters are taken into account in this procedure. The maximal differences relative to the nominal results are taken as a measure of the associated systematic uncertainty. These studies result in a relative uncertainty of less than 2.6% on the extracted jet-gap-jet fractions.

A summary of the systematic uncertainties is presented in Table 1. The systematic uncertainties are added in quadrature and the total bin specific systematic uncertainty varies between 7% and 22%.

8.2 Systematic uncertainties in study of proton-gap-jet-gap-jet events

In addition to the sources of systematic uncertainties described in Section 8.1, the following sources of systematic uncertainties that affect the extraction of the proton-gap-jet-gap-jet fraction f_{CSE} are considered:

- **NBD fit interval:** Because of the limited sample size, the NBD function fit is loosely constrained in the control region, and the extrapolation used to estimate the number of color exchange dijet events in the low multiplicity bins becomes more sensitive to the chosen N_{Tracks} fit interval. The color exchange dijet background for intervals of

Table 1: Relative systematic uncertainties in percentage for the measurements of f_{CSE} in jet-gap-jet events and proton-gap-jet-gap-jet events. The jet-gap-jet results summarize the systematic uncertainties found in bins of the kinematic variables of interest $p_{\mathrm{T,\,jet\text{-}2}}$, $\Delta\eta_{\mathrm{jj}}$, and $\Delta\phi_{\mathrm{jj}}$. When an uncertainty range is given, the range of values is representative of the variation found in the jet-gap-jet fraction in bins of the kinematic variables of interest.

Source	Jet-gap-jet			Proton-gap-jet-gap-jet
	$\Delta\eta_{\mathrm{jj}}$	$p_{\mathrm{T,\,jet\text{-}2}}$	$\Delta\phi_{\mathrm{jj}}$	
Jet energy scale	1.0–5.0	1.5–6.0	0.5–3.0	0.7
Track quality criteria	6.0–8.0	5.4–8.0	1.5–8.0	8
Charged particle p_{T} threshold	2.0–5.8	1.6–4.0	1.1–5.8	11
Background subtraction method	4.7–14.6	2–14.6	12.0	28.3
NBD fit parameter	0.8–2.6	0.6–1.7	0.1–0.6	7
NBD fit interval	—	—	—	12.0
Calorimeter energy scale	—	—	—	5.0
Horizontal dispersion	—	—	—	6.0
Fiducial selection requirements	—	—	—	2.6
Total	6.8–22.0	8.3–14.9	12.0–17.1	33.4

$2 \leq N_{\mathrm{Tracks}} \leq 15$ and $2 \leq N_{\mathrm{Tracks}} \leq 35$ is evaluated. The difference of the extracted gap fraction for these intervals relative to the nominal fit interval $2 \leq N_{\mathrm{Tracks}} \leq 25$ is taken as the associated systematic uncertainty. Based on these studies an uncertainty of 12% is assigned to the extracted gap fraction. The difference of the extracted gap fraction using the fit interval $3 \leq N_{\mathrm{Tracks}} \leq 25$ relative to the nominal fit interval is found to be negligible.

- **Calorimeter energy scale uncertainty:** Beam background contributions are suppressed via the requirement $\xi_p(\mathrm{PF}) - \xi_p(\mathrm{RP}) < 0$ in the analysis. Since $\xi_p(\mathrm{PF})$ is reconstructed from the PF candidates of the CMS experiment, it is affected by the energy-calibration uncertainties of each PF candidates. The impact on $\xi_p(\mathrm{PF})$ is estimated by varying the energy of the PF candidates conservatively by $\pm 10\%$ [60]. The corresponding relative difference in the extracted gap fraction is 5%, and is included as the associated systematic uncertainty.
- **Horizontal dispersion uncertainty:** The reconstruction of $\xi_p(\mathrm{RP})$ depends on the LHC optics parametrization in the transport matrix, which connects the kinematics of the proton at the interaction point with the ones measured at the RPs. The horizontal dispersion term in the transport matrix directly affects the measurement of $\xi_p(\mathrm{RP})$ [57]. The associated systematic uncertainty is estimated by conservatively scaling the value of $\xi_p(\mathrm{RP})$ by $\pm 10\%$, and repeating the analysis. The respective relative uncertainty has a value of 6% on the proton-gap-jet-gap-jet fraction.
- **Fiducial selection requirements for $x - y$ coordinates at the RPs:** The vertical and horizontal fiducial requirements are varied by 200 μm and 1 mm, respectively. The size of these variations are representative of the uncertainties related to the RP alignment [66]. The relative difference with respect to the nominal fiducial $x - y$ requirements on the extraction of the gap fraction is less than 2.6%, and is assigned as the respective systematic uncertainty.

The results of these systematic uncertainties are summarized in Table 1. The total systematic uncertainty is calculated as the quadratic sum of the individual contributions, and is found to have a value of 33.4%.

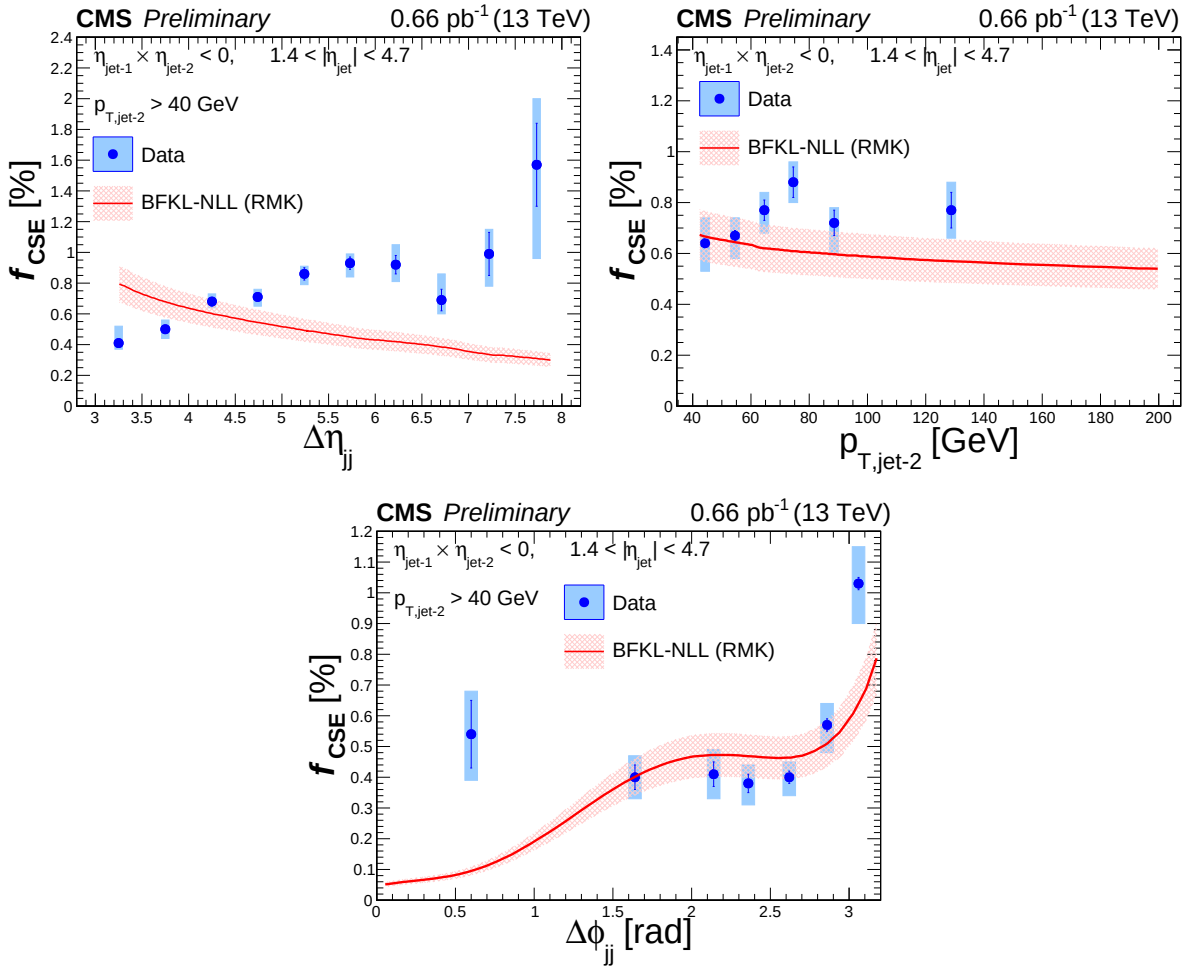

Figure 8: Fraction of color singlet exchange dijet events, f_{CSE}, measured as a function of $\Delta\eta_{\mathrm{jj}}$, $p_{\mathrm{T,jet\text{-}2}}$, and $\Delta\phi_{\mathrm{jj}}$ in pp collisions at $\sqrt{s} = 13$ TeV. Vertical bars represent statistical uncertainties, while boxes represent the combination of statistical and systematic uncertainties in quadrature. The results are plotted at the mean values of $\Delta\eta_{\mathrm{jj}}$, $p_{\mathrm{T,\,jet\text{-}2}}$, and $\Delta\phi_{\mathrm{jj}}$ in the bin. The results on f_{CSE} versus $\Delta\eta_{\mathrm{jj}}$ and $p_{\mathrm{T,jet\text{-}2}}$ are integrated over $\Delta\phi_{\mathrm{jj}}$. The solid curve corresponds to theoretical predictions by the Royon, Marquet, Kepka (RMK) model [70, 71] with survival probability of $|\mathcal{S}|^2 = 10\%$. The hatched band represents the associated theoretical uncertainties.

9 Results

9.1 Results of jet-gap-jet events in inclusive dijet production

The measured gap fractions are presented in Fig. 8 and Tables 2, 3, 4. Within the experimental uncertainties, f_{CSE} is found to show little, if any, dependence on $p_{\mathrm{T,\,jet\text{-}2}}$, with a value of about 0.7%. As a function of the pseudorapidity difference between the two leading jets, $\Delta\eta_{\mathrm{jj}}$, the f_{CSE} fraction shows a uniform increase from 0.4 to 1% for $\Delta\eta_{\mathrm{jj}}$ between 3 and 6. As a function of the azimuthal angle separation between the leading two jets, $\Delta\phi_{\mathrm{jj}}$, the f_{CSE} fraction shows evidence of a peak near $\Delta\phi_{\mathrm{jj}} = \pi$ with a value of 1%, which suggests that the jet-gap-jet events are more strongly correlated in the transverse plane than inclusive dijets. A constant behavior is found for $\Delta\phi_{\mathrm{jj}} < 2.8$ with a value of around 0.4%. The constant value of f_{CSE} for smaller azimuthal separations implies that jet-gap-jet events decorrelate at a similar rate as for color exchange dijet events for smaller azimuthal separations between the jets.

Table 2: Measured values of the jet-gap-jet fraction f_{CSE} in bins of pseudorapidity difference between the leading two jets $\Delta\eta_{\mathrm{jj}}$. The first column indicates the $\Delta\eta_{\mathrm{jj}}$ intervals and the last column represents the measured fraction. The first and second uncertainties correspond to the statistical and systematic components, respectively. The results are for jets satisfying $p_{\mathrm{T,\,jet}} > 40$ GeV and $0 < \Delta\phi_{\mathrm{jj}} < \pi$. The mean values of $\Delta\eta_{\mathrm{jj}}$ in the bin are given in the middle column.

$\Delta\eta_{\mathrm{jj}}$	$\langle\Delta\eta_{\mathrm{jj}}\rangle$	f_{CSE} [%]
3 – 3.5	3.24	$0.41 \pm 0.02^{+0.11}_{-0.04}$
3.5 – 4	3.75	$0.50 \pm 0.02^{+0.06}_{-0.06}$
4 – 4.5	4.25	$0.68 \pm 0.02^{+0.05}_{-0.03}$
4.5 – 5	4.74	$0.71 \pm 0.03^{+0.04}_{-0.05}$
5 – 5.5	5.24	$0.86 \pm 0.04^{+0.03}_{-0.06}$
5.5 – 6	5.73	$0.93 \pm 0.04^{+0.05}_{-0.08}$
6 – 6.5	6.22	$0.92 \pm 0.06^{+0.11}_{-0.09}$
6.5 – 7	6.71	$0.69 \pm 0.07^{+0.15}_{-0.05}$
7 – 7.5	7.22	$0.99 \pm 0.14^{+0.07}_{-0.15}$
7.5 – 8	7.73	$1.57 \pm 0.27^{+0.34}_{-0.55}$

Table 3: Measured values of the jet-gap-jet fraction f_{CSE} in bins of the subleading jet transverse momentum $p_{\mathrm{T,jet\text{-}2}}$. The first column indicates the $p_{\mathrm{T,jet\text{-}2}}$ bin intervals and the last column represents the measured fraction. The first and second uncertainties correspond to the statistical and systematic components, respectively. The results are for jets satisfying $1.4 < |\eta_{\mathrm{jet}}| < 4.7$ and $0 < \Delta\phi_{\mathrm{jj}} < \pi$. The mean values of $p_{\mathrm{T,jet\text{-}2}}$ in the bin are given in the middle column.

$p_{\mathrm{T,jet\text{-}2}}$ [GeV]	$\langle p_{\mathrm{T,jet\text{-}2}}\rangle$ [GeV]	f_{CSE} [%]
40 – 50	44.3	$0.64 \pm 0.01^{+0.10}_{-0.11}$
50 – 60	54.5	$0.67 \pm 0.02^{+0.07}_{-0.09}$
60 – 70	64.6	$0.77 \pm 0.04^{+0.06}_{-0.08}$
70 – 80	74.5	$0.88 \pm 0.06^{+0.06}_{-0.05}$
80 – 100	88.6	$0.72 \pm 0.05^{+0.04}_{-0.11}$
100 – 200	128.8	$0.77 \pm 0.07^{+0.08}_{-0.09}$

Table 4: Measured values of the jet-gap-jet fraction f_{CSE} in bins of azimuthal angle difference between the leading two jets $\Delta\phi_{\mathrm{jj}}$. The first column indicates the $\Delta\phi_{\mathrm{jj}}$ bin intervals and the last column represents the measured fraction. The first and second uncertainties correspond to the statistical and systematic components, respectively. The results are for jets satisfying $p_{\mathrm{T,\,jet}} > 40$ GeV and $1.4 < |\eta_{\mathrm{jet}}| < 4.7$. The mean values of $\Delta\phi_{\mathrm{jj}}$ in the bin are given in the middle column.

$\Delta\phi_{\mathrm{jj}}$ [rad]	$\langle\Delta\phi_{\mathrm{jj}}\rangle$	f_{CSE} [%]
0 – 1	0.60	$0.54 \pm 0.11^{+0.09}_{-0.10}$
1 – 2	1.64	$0.40 \pm 0.04^{+0.06}_{-0.06}$
2 - 2.25	2.14	$0.41 \pm 0.04^{+0.07}_{-0.07}$
2.25 – 2.5	2.36	$0.38 \pm 0.03^{+0.05}_{-0.06}$
2.5 – 2.75	2.62	$0.40 \pm 0.02^{+0.05}_{-0.06}$
2.75 – 3	2.86	$0.57 \pm 0.02^{+0.07}_{-0.09}$
3 – π	3.06	$1.03 \pm 0.02^{+0.12}_{-0.13}$

As mentioned in Section 5, no neutral particles are used in the definition of the pseudorapidity gap because of the relatively large transverse energy thresholds above calorimeter noise for neutral hadrons and photons. Most dijet events with low charged particle multiplicities in $|\eta| < 1$ are found to have little, if any, neutral particle activity in $|\eta| < 1$. Simulation studies suggest that the neutral hadron and photon activity observed in data originate from the emission of jet constituents into the fixed pseudorapidity interval, together with residual contributions of calorimeter noise. The gap fractions remain mostly unaffected if the contribution of neutral particles in central pseudorapidities is restricted in the analysis. In particular, if the vector sum of neutral hadrons and photons transverse energy in $|\eta| < 1$ is required to be no larger than 15 GeV, the results are found to be the same, within statistical uncertainties. This is consistent with the fact that the color exchange dijet background is already subtracted in the determination of f_{CSE}.

The present results are compared to predictions by Royon, Marquet, and Kepka (RMK model) based on BFKL calculations with resummation of large logarithms of energy at NLL accuracy and with LO impact factors [70, 71], with an updated parametrization to take into account the larger phase space available at the LHC energies [93]. The gap survival probability factor is taken into account as a uniform $|\mathcal{S}|^2 = 10\%$ multiplicative factor in this model. These predictions are presented in Fig. 8. According to these calculations, the gap fraction should have a weak dependence on $p_{\mathrm{T,\,jet\text{-}2}}$. Within uncertainties, this feature is consistent with the observed f_{CSE} values. The model predicts a decreasing f_{CSE} with increasing $\Delta\eta_{\mathrm{jj}}$, in disagreement with the data that shows a gap fraction that generally grows with larger $\Delta\eta_{\mathrm{jj}}$. The predicted jet-gap-jet fractions as a function of $\Delta\phi_{\mathrm{jj}}$ are consistent with the data within uncertainties for medium angular separations $1 < \Delta\phi_{\mathrm{jj}} < 3$ rad, but underestimate the experimental result by around 10% near $\Delta\phi_{\mathrm{jj}} = \pi$. The model significantly underestimates the observed f_{CSE} for small angular separations with $\Delta\phi_{\mathrm{jj}} < 1$.

The present disagreement between theory and data indicate the need for a better understanding of central rapidity gap formation and destruction mechanisms. Present calculations include partial next-to-leading order (NLO) corrections within the BFKL framework. Recently, major improvements have been presented in the calculation of NLO impact factors for the jet-gap-jet process [94, 95]. It is possible that if predictions include these corrections, together with the resummation of large logarithms of energy at NLL in BFKL, the tension between theory and data could decrease. An improved description of nonperturbative survival probability effects is also necessary.

In Fig. 9 the current results are compared with previous measurements of the gap fraction f_{CSE} with a fixed central pseudorapidity gap in $|\eta| < 1$ by the D0 and CDF Collaborations at the Tevatron in $\mathrm{p\bar{p}}$ collisions at the collision energies of $\sqrt{s} = 0.63$ and 1.8 TeV [39, 40, 42, 43], and by the CMS Collaboration in pp collisions at $\sqrt{s} = 7$ TeV [44]. There are differences on the phase space volumes occupied by the leading two jets, jet clustering algorithms and distance parameters, which are described in the next paragraphs. Simulation studies that rely on generator-level particle distributions indicate that the choice of the jet reconstruction algorithm, i.e. cone or anti-k_{T} algorithm, has a negligible effect on the shape of the multiplicity distribution. The value of the distance parameter R influences the charged particle multiplicity distribution shape of jet-gap-jet signal events. For large values of R, it is less likely for charged particle constituents of the jet to populate the fixed pseudorapidity interval since the jet axes are further away from the edges of the gap region. This yields a sharper jet-gap-jet signal excess at $N_{\mathrm{Tracks}} = 0$ for large jet radius. At small distance parameter R, there is more spillage of charged particles into the gap region, since the jet axes can approach the edge of the fixed pseudorapidity interval more closely. The shape of the multiplicity distribution of color ex-

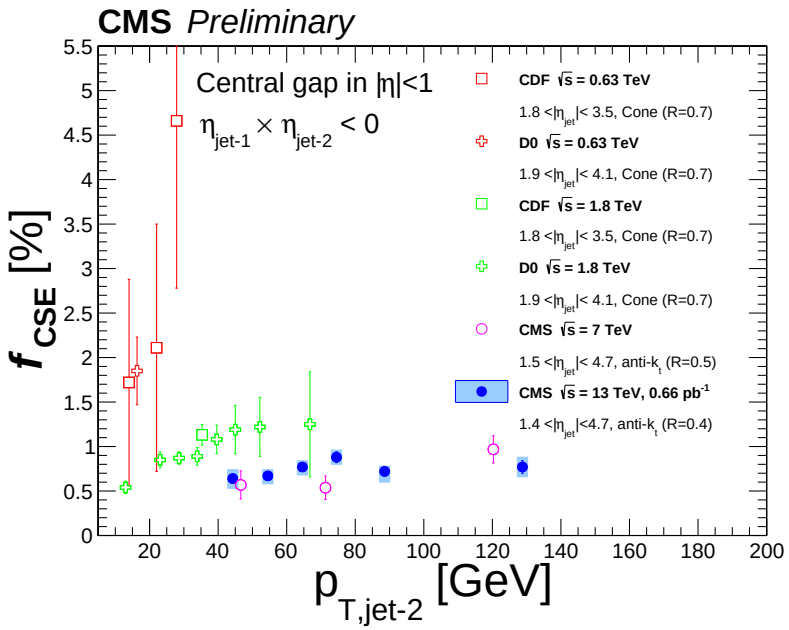

Figure 9: Fraction of color singlet exchange dijet events, f_{CSE}, measured as a function of the subleading jet transverse momentum $p_{\mathrm{T,jet\text{-}2}}$ by the D0 and CDF Collaborations [40, 42, 43] at $\sqrt{s} = 0.63$ (red symbols) and 1.8 TeV (green symbols), and by the CMS Collaboration [44] at 7 TeV (magenta symbol) and the present results at 13 TeV (blue band). The central gap is defined by means of the particle activity in the fixed pseudorapidity interval $|\eta| < 1$ in these measurements.

change dijet events remains mostly unaffected by the size of R. In these simulation studies, these effects are found to be negligible provided that the jet-gap-jet fraction is extracted over the first multiplicity bins $N_{\mathrm{Tracks}} < 3$, as is done in this measurement.

The study by the D0 Collaboration [40] uses the calorimeter tower multiplicity distribution in $|\eta| < 1$, where the transverse energy of each calorimeter tower has a value of $E_{\mathrm{T}} > 200$ MeV. The 0.63 and 1.8 TeV studies consider jets with $E_{\mathrm{T,\,jet\text{-}2}} > 12$ GeV and $1.9 < |\eta_{\mathrm{jet}}| < 4.1$. The CDF Collaboration studies jet-gap-jet events at 0.63 and 1.8 TeV [42, 43]. The multiplicity of charged particles between the jets in $|\eta| < 1$ with transverse energies of $E_{\mathrm{T}} > 300$ MeV is used in these studies. Each of the two leading jets has pseudorapidities of $1.8 < |\eta_{\mathrm{jet}}| < 3.5$, and transverse energy of $E_{\mathrm{T,\,jet\text{-}2}} > 8$ GeV and $E_{\mathrm{T,\,jet\text{-}2}} > 20$ GeV for the 0.63 and 1.8 TeV studies, respectively. The jets are clustered with the cone algorithm with distance parameter $R = 0.7$ for both CDF and D0 studies. The measurement by CMS at 7 TeV is done in three bins of $p_{\mathrm{T,\,jet\text{-}2}} = 40$–60, 60–100, and 100–200 GeV [44]. The jets are clustered with the anti-k_{T} algorithm with a distance parameter of 0.5. Each of the leading two jets has pseudorapidity of $1.5 < |\eta_{\mathrm{jet}}| < 4.7$, and the signal extraction is based on the multiplicity distribution of charged particle tracks with $p_{\mathrm{T}} > 200$ GeV in $|\eta| < 1$.

Referring to Fig. 9, the D0 and CDF Collaborations find that the fraction of jet-gap-jet events decreases by a factor of 2.5 ± 0.9 [40] and 3.4 ± 1.2 [43], respectively, when $\sqrt{s}$ increases from 0.63 to 1.8 TeV. Similarly, the results by the CMS experiment at 7 TeV show a gap fraction that decreases by a factor of around 2 with respect to the 1.8 TeV results at the Tevatron [44]. The observed energy dependence of the previous measurements is generally attributed to a larger number of soft parton interactions with increasing $\sqrt{s}$, which enhances the probability of the gap being destroyed. The 13 TeV results show there is no further decrease of the gap fraction

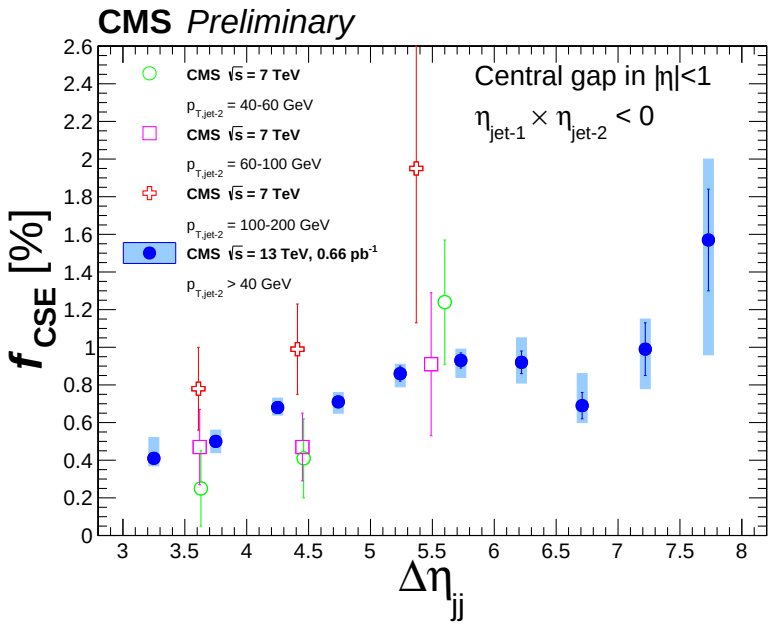

Figure 10: Fraction of color singlet exchange dijet events, f_{CSE}, measured as a function of $\Delta\eta_{\mathrm{jj}}$ by CMS at 7 TeV [44] and the present measurement at 13 TeV. The 7 TeV measurement was performed in three bins of the transverse momentum of the subleading jet $p_{\mathrm{T,\,jet\text{-}2}} = 40$–$60$, 60–100, 100–200 GeV, which are represented by the open circle, square, and cross symbols, respectively.

values relative to the 7 TeV results, within uncertainties. This could be an indication that the rapidity gap survival probability stops decreasing at the collision energies probed at the LHC for the jet-gap-jet process.

The f_{CSE} value as a function of $\Delta\eta_{\mathrm{jj}}$ expands the reach in pseudorapidity separations covered in the earlier 7 TeV CMS measurement, as seen in Fig. 10. The measurement of the gap fraction as a function of $\Delta\eta_{\mathrm{jj}}$ at 7 TeV is done in three bins of pseudorapidity separations $\Delta\eta_{\mathrm{jj}} = 3$–$4$, 4–5, 5–7 units for each bin of $p_{\mathrm{T,\,jet\text{-}2}}$. The dependence of the jet-gap-jet fraction as a function of $\Delta\eta_{\mathrm{jj}}$ at 13 TeV confirms the trend observed by CMS at 7 TeV, and extends the range previously explored towards large values of $\Delta\eta_{\mathrm{jj}}$.

9.2 Results of jet-gap-jet events with a leading proton

The ratio of proton-gap-jet-gap-jet events to proton-gap-jet-jet events is $f_{\mathrm{CSE}} = 1.92 \pm 0.46$ (stat) $^{+0.66}_{-0.58}$ (syst) %. Most of the events with leading protons considered here have separations $3 < \Delta\eta_{\mathrm{jj}} < 6.5$ and subleading jet transverse momentum $40 < p_{\mathrm{T,jet\text{-}2}} < 100$ GeV. The jet-gap-jet fraction in events with a leading proton is found to be 2.91 ± 0.70 (stat) $^{+1.02}_{-0.94}$ (syst) times larger than that extracted for inclusive dijet production, where the leading two jets have similar kinematics as those in the study with an intact proton ($40 < p_{\mathrm{T,\,jet\text{-}2}} < 100$ GeV and $3 < \Delta\eta_{\mathrm{jj}} < 6.5$). The gap fraction in the latter jet-gap-jet subsample has a value of $f_{\mathrm{CSE}} = 0.66 \pm 0.01$ (stat) $^{+0.05}_{-0.08}$ (syst) %. Correlations of systematic uncertainties associated with jet reconstruction and central gap definition are taken into account when evaluating the uncertainties in the double-ratios. Statistical and systematic uncertainties in the double-ratio are largely dominated by the uncertainties in the CMS-TOTEM f_{CSE} measurement. The CMS-TOTEM results, when compared to the CMS results, suggest that the relative abundance of dijet events with a central gap is larger in events with a leading proton, as shown in Fig. 11 where the gap fraction f_{CSE} is presented as

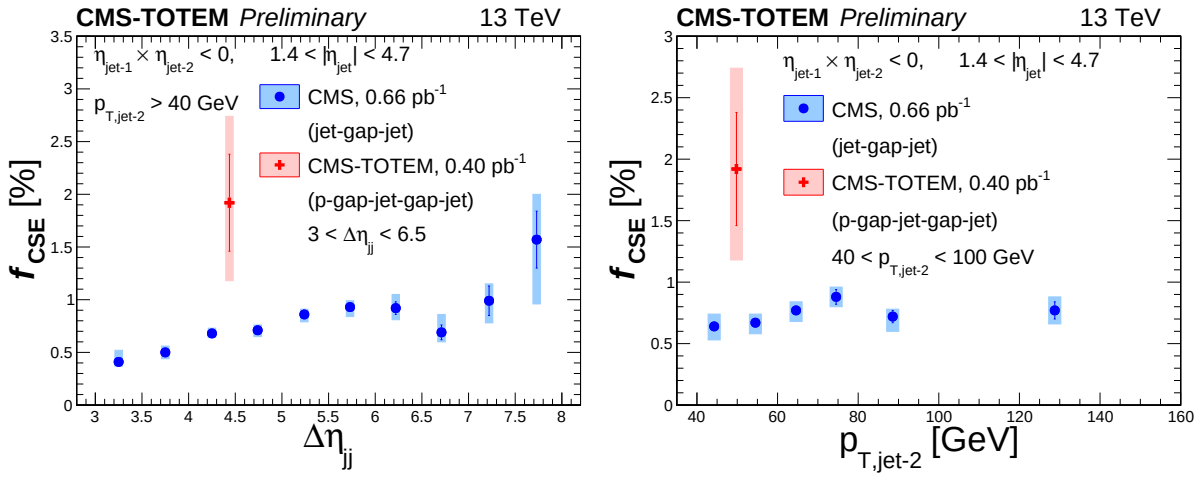

Figure 11: Gap fraction, f_{CSE}, measured as a function of $\Delta\eta_{\mathrm{jj}}$ and $p_{\mathrm{T,\,jet\text{-}2}}$ in inclusive dijet event production (labeled CMS, represented by the circle marker) and in dijet events with a leading proton at 13 TeV (labeled CMS-TOTEM, represented by the cross marker). Vertical bars represent statistical uncertainties, while boxes represent the combination of statistical and systematic uncertainties in quadrature. The CMS-TOTEM results are plotted at the mean values of $\Delta\eta_{\mathrm{jj}}$ and $p_{\mathrm{T,\,jet\text{-}2}}$ in the bin. Most of the CMS-TOTEM events considered here have separations $3 < \Delta\eta_{\mathrm{jj}} < 6.5$, and transverse momenta $40 < p_{\mathrm{T,\,jet\text{-}2}} < 100$ GeV, as indicated in the figure.

a function of $\Delta\eta_{\mathrm{jj}}$ and $p_{\mathrm{T,\,jet\text{-}2}}$.

The larger gap fraction in events with a leading proton allows for an interpretation in terms of a reduced spectator parton activity in reactions with an intact proton in comparison to the soft parton activity in interactions where the proton breaks up. In the latter, there can be soft parton exchanges between the proton remnants and partons produced in the collision, which can destroy the central gap signature between the final-state jets. A similar effect has been observed in other diffractive topologies in dijet events with two rapidity gaps by the CDF Collaboration at $\sqrt{s} = 1.8$ TeV [96], where a comparison is made of the ratio of yields of single-diffractive dijet events to non-diffractive dijet events, $R^{\mathrm{SD}}_{\mathrm{ND}}$, and the ratio of double-pomeron exchange dijet events to single-diffractive dijet events, $R^{\mathrm{DPE}}_{\mathrm{SD}}$, and finding that the double-ratio has a value of $R^{\mathrm{SD}}_{\mathrm{ND}}/R^{\mathrm{DPE}}_{\mathrm{SD}} = 0.19 \pm 0.07$ [96]. This suggests that a gap is more likely to form or survive in presence of another gap. An equivalent double-ratio definition for the present measurement is $f_{\mathrm{CSE}}(\text{jet-gap-jet})/f_{\mathrm{CSE}}(\text{p-gap-jet-gap-jet}) = 0.34 \pm 0.08\,(\text{stat})\,^{+0.11}_{-0.12}\,(\text{syst})$, which is observed to be of similar size as that for a double-pomeron exchange dijet topology reported by the CDF Collaboration.

Although there are no explicit predictions for jet-gap-jet events with a leading proton, calculations based on the BFKL framework at NLL accuracy for jet-gap-jet events with two leading protons predict gap fractions of the order of 15 – 20% [56]. These calculations assume factorization of the survival probability. The present measurement sets a constraint on the theoretical treatment of rapidity gap survival probability.

10 Summary

Events with two leading jets separated by a large pseudorapidity gap have been studied in pp collisions at $\sqrt{s} = 13$ TeV with the CMS detector. The "gap" is determined by the absence of charged particles with $p_{\mathrm{T}} > 200$ MeV in the pseudorapidity range $|\eta| < 1$ produced in the

collision. Each of the two leading jets has pseudorapidity values of $1.4 < |\eta_{\text{jet}}| < 4.7$ and transverse momentum of $p_{\text{T, jet}} > 40$ GeV, with $\eta_{\text{jet-1}} \times \eta_{\text{jet-2}} < 0$. The pseudorapidity gap signature is indicative of an underlying hard color singlet exchange, which is described in terms of two-gluon exchange in perturbative quantum chromodynamics. Jet-gap-jet events appear as an excess of events over the expected charged particle multiplicity of color exchange dijet events at the lowest charged particle multiplicity counts. The fraction of jet-gap-jet events to events where the two jets have similar kinematics, f_{CSE}, has been measured as a function of the pseudorapidity difference between the leading two jets, $\Delta\eta_{\text{jj}} \equiv |\eta_{\text{jet-1}} - \eta_{\text{jet-2}}|$, the transverse momentum of the subleading jet, $p_{\text{T, jet-2}}$, and the azimuthal angle separation between the leading two jets, $\Delta\phi_{\text{jj}} \equiv |\phi_{\text{jet-1}} - \phi_{\text{jet-2}}|$.

The fraction f_{CSE} has values of 0.6–1%. It increases with $\Delta\eta_{\text{jj}}$, is only weakly dependent on $p_{\text{T, jet-2}}$, and increases as $\Delta\phi_{\text{jj}}$ approaches π. No significant difference in f_{CSE} is observed comparing the present results at 13 TeV with those presented by the CMS Collaboration at 7 TeV. This is in contrast to the trend found at lower collision energies of 0.63 and 1.8 TeV by the D0 and CDF Collaborations, where a significant decrease with increasing energy was observed. The results are compared with calculations based on the Balitsky–Fadin–Kuraev–Lipatov framework with resummation of large logarithms of energy at next-to-leading logarithm accuracy, leading order impact factors, and a constant survival probability factor. The implementation by Royon, Marquet, and Kepka describes some features of the data, but is not able to simultaneously describe all aspects of the measurement. The present disagreement between theory and data provides guidance for further improvements on the perturbative and nonperturbative treatment for pseudorapidity gap formation and destruction mechanisms.

Complementary to the jet-gap-jet study, a sample of dijet events with leading protons collected by the CMS and TOTEM experiments in 2015 is used to study jet-gap-jet events with leading protons, which correspond to proton-gap-jet-gap-jet topologies. This is the first study of this diffractive event topology. The gap fraction extracted in this sample is found to be 2.91 ± 0.70 (stat) $^{+1.02}_{-0.94}$ (syst) times larger than that found in inclusive dijet production, pointing to a larger abundance of jets with a central gap in events with leading protons. This can be interpreted in terms of a lower spectator parton activity in events with leading protons, which decreases the likelihood of the central gap signature being spoiled.

References

[1] Particle Data Group Collaboration, "Review of Particle Physics", *Phys. Rev. D* **98** (2018) 030001, doi:10.1103/PhysRevD.98.030001.

[2] E. A. Kuraev, L. N. Lipatov, and V. S. Fadin, "The Pomeranchuk singularity in nonabelian gauge theories", *Sov. Phys. JETP* **45** (1977) 199.

[3] I. I. Balitsky and L. N. Lipatov, "The Pomeranchuk singularity in quantum chromodynamics", *Sov. J. Nucl. Phys.* **28** (1978) 822.

[4] L. N. Lipatov, "The bare pomeron in quantum chromodynamics", *Sov. Phys. JETP* **63** (1986) 904.

[5] V. S. Fadin and L. N. Lipatov, "BFKL pomeron in the next-to-leading approximation", *Phys. Lett. B* **429** (1998) 127, doi:10.1016/S0370-2693(98)00473-0, arXiv:hep-ph/9802290.

[6] M. Ciafaloni and G. Camici, "Energy scale(s) and next-to-leading BFKL equation", *Phys. Lett. B* **430** (1998) 349, doi:10.1016/S0370-2693(98)00551-6, arXiv:hep-ph/9803389.

[7] CMS Collaboration, "Azimuthal decorrelation of jets widely separated in rapidity in pp collisions at $\sqrt{s} = 7$ TeV", *JHEP* **08** (2016) 139, doi:10.1007/JHEP08(2016)139, arXiv:1601.06713.

[8] LHCb Collaboration, "Updated measurements of exclusive J/ψ and ψ(2S) production cross-sections in pp collisions at $\sqrt{s} = 7$ TeV", *J. Phys. G* **41** (2014) 055002, doi:10.1088/0954-3899/41/5/055002, arXiv:1401.3288.

[9] LHCb Collaboration, "Measurement of the exclusive Y production cross-section in pp collisions at $\sqrt{s} = 7$ TeV and 8 TeV", *JHEP* **09** (2015) 084, doi:10.1007/JHEP09(2015)084, arXiv:1505.08139.

[10] ALICE Collaboration, "Coherent J/ψ photoproduction in ultra-peripheral Pb-Pb collisions at $\sqrt{s_{NN}} = 2.76$ TeV", *Phys. Lett. B* **718** (2013) 1273, doi:10.1016/j.physletb.2012.11.059, arXiv:1209.3715.

[11] ALICE Collaboration, "Exclusive J/ψ photoproduction off protons in ultra-peripheral p-Pb collisions at $\sqrt{s_{\rm NN}} = 5.02$ TeV", *Phys. Rev. Lett.* **113** (2014) 232504, doi:10.1103/PhysRevLett.113.232504, arXiv:1406.7819.

[12] ALICE Collaboration, "Coherent ρ^0 photoproduction in ultra-peripheral Pb-Pb collisions at $\sqrt{s_{\rm NN}} = 2.76$ TeV", *JHEP* **09** (2015) 095, doi:10.1007/JHEP09(2015)095, arXiv:1503.09177.

[13] CMS Collaboration, "Measurement of exclusive Y photoproduction from protons in pPb collisions at $\sqrt{s_{\rm NN}} = 5.02$ TeV", *Eur. Phys. J. C* **79** (2019) 277, doi:10.1140/epjc/s10052-019-6774-8, arXiv:1809.11080.

[14] CMS Collaboration, "Measurement of exclusive $\rho(770)^0$ photoproduction in ultraperipheral pPb collisions at $\sqrt{s_{\rm NN}} = 5.02$ TeV", *Eur. Phys. J. C* **79** (2019) 702, doi:10.1140/epjc/s10052-019-7202-9, arXiv:1902.01339.

[15] V. N. Gribov and L. N. Lipatov, "Deep inelastic ep scattering in perturbation theory", *Sov. J. Nucl. Phys.* **15** (1972) 438.

[16] G. Altarelli and G. Parisi, "Asymptotic freedom in parton language", *Nucl. Phys. B* **126** (1977) 298, doi:10.1016/0550-3213(77)90384-4.

[17] Y. L. Dokshitzer, "Calculation of the structure functions for deep inelastic scattering and e^+ e^- annihilation by perturbation theory in quantum chromodynamics", *Sov. Phys. JETP* **46** (1977) 641.

[18] CMS Collaboration, "Measurement of the differential dijet production cross section in proton-proton collisions at $\sqrt{s} = 7$ TeV", *Phys. Lett. B* **700** (2011) 187, doi:10.1016/j.physletb.2011.05.027, arXiv:1104.1693.

[19] CMS Collaboration, "Measurement of the inclusive production cross sections for forward jets and for dijet events with one forward and one central jet in pp collisions at $\sqrt{s} = 7$ TeV", *JHEP* **06** (2012) 036, doi:10.1007/JHEP06(2012)036, arXiv:1202.0704.

[20] CMS Collaboration, "Ratios of dijet production cross sections as a function of the absolute difference in rapidity between jets in proton-proton collisions at $\sqrt{s} = 7$ TeV", *Eur. Phys. J. C* **72** (2012) 2216, doi:10.1140/epjc/s10052-012-2216-6, arXiv:1204.0696.

[21] CMS Collaboration, "Measurement of the inclusive jet cross section in pp collisions at $\sqrt{s} = 2.76$ TeV", *Eur. Phys. J. C* **76** (2016) 265, doi:10.1140/epjc/s10052-016-4083-z, arXiv:1512.06212.

[22] CMS Collaboration, "Measurement of dijet azimuthal decorrelation in pp collisions at $\sqrt{s} = 8$ TeV", *Eur. Phys. J. C* **76** (2016) 536, doi:10.1140/epjc/s10052-016-4346-8, arXiv:1602.04384.

[23] CMS Collaboration, "Measurement of the double-differential inclusive jet cross section in proton-proton collisions at $\sqrt{s} = 13$ TeV", *Eur. Phys. J. C* **76** (2016) 451, doi:10.1140/epjc/s10052-016-4286-3, arXiv:1605.04436.

[24] CMS Collaboration, "Measurement and QCD analysis of double-differential inclusive jet cross sections in pp collisions at $\sqrt{s} = 8$ TeV and cross section ratios to 2.76 and 7 TeV", *JHEP* **03** (2017) 156, doi:10.1007/JHEP03(2017)156, arXiv:1609.05331.

[25] CMS Collaboration, "Azimuthal correlations for inclusive 2-jet, 3-jet, and 4-jet events in pp collisions at $\sqrt{s} = 13$ TeV", *Eur. Phys. J. C* **78** (2018) 566, doi:10.1140/epjc/s10052-018-6033-4, arXiv:1712.05471.

[26] CMS Collaboration, "Measurement of inclusive very forward jet cross sections in proton-lead collisions at $\sqrt{s_{\mathrm{NN}}} = 5.02$ TeV", *JHEP* **05** (2019) 043, doi:10.1007/JHEP05(2019)043, arXiv:1812.01691.

[27] ATLAS Collaboration, "Measurement of inclusive jet and dijet cross sections in proton-proton collisions at 7 TeV centre-of-mass energy with the ATLAS detector", *Eur. Phys. J. C* **71** (2011) 1512, doi:10.1140/epjc/s10052-010-1512-2, arXiv:1009.5908.

[28] ATLAS Collaboration, "Measurement of dijet production with a veto on additional central jet activity in pp collisions at $\sqrt{s} = 7$ TeV using the ATLAS detector", *JHEP* **09** (2011) 053, doi:10.1007/JHEP09(2011)053, arXiv:1107.1641.

[29] ATLAS Collaboration, "Measurement of inclusive jet and dijet production in pp collisions at $\sqrt{s} = 7$ TeV using the ATLAS detector", *Phys. Rev. D* **86** (2012) 014022, doi:10.1103/PhysRevD.86.014022, arXiv:1112.6297.

[30] ATLAS Collaboration, "Measurement of dijet cross sections in pp collisions at 7 TeV centre-of-mass energy using the ATLAS detector", *JHEP* **05** (2014) 059, doi:10.1007/JHEP05(2014)059, arXiv:1312.3524.

[31] ATLAS Collaboration, "Measurements of jet vetoes and azimuthal decorrelations in dijet events produced in pp collisions at $\sqrt{s} = 7$ TeV using the ATLAS detector", *Eur. Phys. J. C* **74** (2014) 3117, doi:10.1140/epjc/s10052-014-3117-7, arXiv:1407.5756.

[32] ATLAS Collaboration, "Measurement of the inclusive jet cross-sections in proton-proton collisions at $\sqrt{s} = 8$ TeV with the ATLAS detector", *JHEP* **09** (2017) 020, doi:10.1007/JHEP09(2017)020, arXiv:1706.03192.

[33] ATLAS Collaboration, "Measurement of dijet azimuthal decorrelations in pp collisions at $\sqrt{s} = 8$ TeV with the ATLAS detector and determination of the strong coupling", *Phys. Rev. D* **98** (2018) 092004, doi:10.1103/PhysRevD.98.092004, arXiv:1805.04691.

[34] R. D. Ball et al., "Parton distributions with small-x resummation: evidence for BFKL dynamics in HERA data", *Eur. Phys. J. C* **78** (2018) 321, doi:10.1140/epjc/s10052-018-5774-4, arXiv:1710.05935.

[35] A. Mueller and W.-K. Tang, "High energy parton-parton elastic scattering in QCD", *Phys. Lett. B* **284** (1992) 123, doi:10.1016/0370-2693(92)91936-4.

[36] H1 Collaboration, "Energy flow and rapidity gaps between jets in photoproduction at HERA", *Eur. Phys. J. C* **24** (2002) 517, doi:10.1007/s10052-002-0988-9, arXiv:hep-ex/0203011.

[37] ZEUS Collaboration, "Rapidity gaps between jets in photoproduction at HERA", *Phys. Lett. B* **369** (1996) 55, doi:10.1016/0370-2693(95)01588-4, arXiv:hep-ex/9510012.

[38] D0 Collaboration, "Rapidity gaps between jets in $p\bar{p}$ collisions at $\sqrt{s} = 1.8$ TeV", *Phys. Rev. Lett.* **72** (1994) 2332, doi:10.1103/PhysRevLett.72.2332.

[39] D0 Collaboration, "Jet production via strongly-interacting color-singlet exchange in $p\bar{p}$ collisions", *Phys. Rev. Lett.* **76** (1996) 734, doi:10.1103/PhysRevLett.76.734, arXiv:hep-ex/9509013.

[40] D0 Collaboration, "Probing hard color-singlet exchange in $p\bar{p}$ collisions at $\sqrt{s} = 630$ GeV and 1800 GeV", *Phys. Lett. B* **440** (1998) 189, doi:10.1016/S0370-2693(98)01238-6, arXiv:hep-ex/9809016.

[41] CDF Collaboration, "Observation of rapidity gaps in $\bar{p}p$ collisions at 1.8 TeV", *Phys. Rev. Lett.* **74** (1995) 855, doi:10.1103/PhysRevLett.74.855.

[42] CDF Collaboration, "Dijet production by color-singlet exchange at the Fermilab Tevatron", *Phys. Rev. Lett.* **80** (1998) 1156, doi:10.1103/PhysRevLett.80.1156.

[43] CDF Collaboration, "Events with a rapidity gap between jets in $\bar{p}p$ collisions at $\sqrt{s} = 630$ GeV", *Phys. Rev. Lett.* **81** (1998) 5278, doi:10.1103/PhysRevLett.81.5278.

[44] CMS Collaboration, "Study of dijet events with a large rapidity gap between the two leading jets in pp collisions at $\sqrt{s} = 7$ TeV", *Eur. Phys. J. C* **78** (2018) 242, doi:10.1140/epjc/s10052-018-5691-6, arXiv:1710.02586.

[45] J. D. Bjorken, "Rapidity gaps and jets as a new-physics signature in very-high-energy hadron-hadron collisions", *Phys. Rev. D* **47** (1993) 101, doi:10.1103/PhysRevD.47.101.

[46] V. Barone and E. Predazzi, "High-energy particle diffraction". Springer, Berlin, 2002. doi:10.1007/978-3-662-04724-8.

[47] S. Donnachie, G. Dosch, P. Landshoff, and O. Nachtmann, "Pomeron physics and QCD". Cambridge Monographs on Particle Physics, Nuclear Physics and Cosmology. Cambridge University Press, 2002. doi:10.1017/CBO9780511534935.

[48] J. R. Forshaw and D. A. Ross, "Quantum chromodynamics and the pomeron". Cambridge Lecture Notes in Physics. Cambridge University Press, 1997. doi:10.1017/CBO9780511524387.

[49] J. Bjorken, "A full-acceptance detector for SSC physics at low and intermediate mass scales: an expression of interest to the SSC", *International Journal of Modern Physics A* **07** (1992) 4189, doi:10.1142/S0217751X92001885.

[50] E. Gotsman, E. Levin, and U. Maor, "Energy dependence of the survival probability of large rapidity gaps", *Phys. Lett. B* **438** (1998) 229, doi:10.1016/S0370-2693(98)00972-1, arXiv:hep-ph/9804404.

[51] V. A. Khoze, A. D. Martin, and M. G. Ryskin, "Diffraction at the LHC", *Eur. Phys. J. C* **73** (2013) 2503, doi:10.1140/epjc/s10052-013-2503-x, arXiv:1306.2149.

[52] E. Gotsman, E. Levin, and U. Maor, "CGC/saturation approach for soft interactions at high energy: survival probability of central exclusive production", *Eur. Phys. J. C* **76** (2016) 177, doi:10.1140/epjc/s10052-016-4014-z, arXiv:1510.07249.

[53] V. A. Khoze, A. D. Martin, and M. G. Ryskin, "Multiple interactions and rapidity gap survival", *J. Phys. G* **45** (2018) 053002, doi:10.1088/1361-6471/aab1bf, arXiv:1710.11505.

[54] R. Enberg, G. Ingelman, and L. Motyka, "Hard color singlet exchange and gaps between jets at the Tevatron", *Phys. Lett. B* **524** (2002) 273, doi:10.1016/S0370-2693(01)01379-X, arXiv:hep-ph/0111090.

[55] I. Babiarz, R. Staszewski, and A. Szczurek, "Multi-parton interactions and rapidity gap survival probability in jet-gap-jet processes", *Phys. Lett. B* **771** (2017) 532, doi:10.1016/j.physletb.2017.05.095, arXiv:1704.00546.

[56] C. Marquet, C. Royon, M. Trzebiński, and R. Žlebčík, "Gaps between jets in double-Pomeron-exchange processes at the LHC", *Phys. Rev. D* **87** (2013) 034010, doi:10.1103/PhysRevD.87.034010, arXiv:1212.2059.

[57] TOTEM Collaboration, "The TOTEM experiment at the CERN Large Hadron Collider", *Journal of Instrumentation* **3** (2008) S08007, doi:10.1088/1748-0221/3/08/s08007.

[58] O. S. Bröning et al., "LHC design report". CERN Yellow Reports: Monographs. CERN, 2004. doi:10.5170/CERN-2004-003-V-1.

[59] CMS Collaboration, "Description and performance of track and primary-vertex reconstruction with the CMS tracker", *JINST* **9** (2014) P10009, doi:10.1088/1748-0221/9/10/P10009, arXiv:1405.6569.

[60] CMS Collaboration, "Particle-flow reconstruction and global event description with the CMS detector", *JINST* **12** (2017) P10003, doi:10.1088/1748-0221/12/10/P10003, arXiv:1706.04965.

[61] M. Cacciari, G. P. Salam, and G. Soyez, "The anti-k_t jet clustering algorithm", *JHEP* **04** (2008) 063, doi:10.1088/1126-6708/2008/04/063, arXiv:0802.1189.

[62] M. Cacciari, G. P. Salam, and G. Soyez, "FastJet user manual", *Eur. Phys. J. C* **72** (2012) 1896, doi:10.1140/epjc/s10052-012-1896-2, arXiv:1111.6097.

[63] CMS Collaboration, "Jet energy scale and resolution in the CMS experiment in pp collisions at 8 TeV", *JINST* **12** (2017) P02014, doi:10.1088/1748-0221/12/02/P02014, arXiv:1607.03663.

[64] CMS Collaboration, "The CMS experiment at the CERN LHC", *JINST* **3** (2008) S08004, doi:10.1088/1748-0221/3/08/S08004.

[65] TOTEM Collaboration, "LHC optics measurement with proton tracks detected by the Roman pots of the TOTEM experiment", *New J. Phys.* **16** (2014) 103041, doi:10.1088/1367-2630/16/10/103041, arXiv:1406.0546.

[66] TOTEM Collaboration, "Performance of the TOTEM detectors at the LHC", *Int. J. Mod. Phys. A* **28** (2013) 1330046, doi:10.1142/S0217751X13300469, arXiv:1310.2908.

[67] H. Niewiadomski, "Reconstruction of protons in the TOTEM Roman pot detectors at the LHC". PhD thesis, Manchester U., 2008. CERN-THESIS-2008-080.

[68] CMS and TOTEM Collaborations, "Measurement of single-diffractive dijet production in proton-proton collisions at $\sqrt{s} = 8$ TeV with the CMS and TOTEM experiments", (2020). arXiv:2002.12146. Submitted to *EPJC*.

[69] B. Cox, J. R. Forshaw, and L. Lönnblad, "Hard color singlet exchange at the Tevatron", *JHEP* **10** (1999) 023, doi:10.1088/1126-6708/1999/10/023, arXiv:hep-ph/9908464.

[70] F. Chevallier, O. Kepka, C. Marquet, and C. Royon, "Gaps between jets at hadron colliders in the next-to-leading BFKL framework", *Phys. Rev. D* **79** (2009) 094019, doi:10.1103/PhysRevD.79.094019, arXiv:0903.4598.

[71] O. Kepka, C. Marquet, and C. Royon, "Gaps between jets in hadronic collisions", *Phys. Rev. D* **83** (2011) 034036, doi:10.1103/PhysRevD.83.034036, arXiv:1012.3849.

[72] A. Giovannini and L. Van Hove, "Negative binomial multiplicity distributions in high energy hadron collisions", *Zeitschrift für Physik C Particles and Fields* **30** (1986) 391, doi:10.1007/BF01557602.

[73] P. Ghosh, "Negative binomial multiplicity distribution in proton-proton collisions in limited pseudorapidity intervals at LHC up to $\sqrt{s} = 7$ TeV and the clan model", *Phys. Rev. D* **85** (2012) 054017, doi:10.1103/PhysRevD.85.054017, arXiv:1202.4221.

[74] UA5 Collaboration, "Multiplicity distributions in different pseudorapidity intervals at a c.o.m. energy of 540 GeV", *Phys. Lett. B* **160** (1985) 193, doi:10.1016/0370-2693(85)91491-1.

[75] UA5 Collaboration, "Charged particle multiplicity distributions at 200 GeV and 900 GeV c.m. energy", *Z. Phys. C* **43** (1989) 357, doi:10.1007/BF01506531.

[76] ALICE Collaboration, "Charged-particle multiplicities in proton-proton collisions at $\sqrt{s} = 0.9$ to 8 TeV", *Eur. Phys. J. C* **77** (2017) 33, doi:10.1140/epjc/s10052-016-4571-1, arXiv:1509.07541.

[77] T. Sjöstrand et al., "An introduction to PYTHIA 8.2", *Comput. Phys. Commun.* **191** (2015) 159, doi:10.1016/j.cpc.2015.01.024, arXiv:1410.3012.

[78] NNPDF Collaboration, "Unbiased global determination of parton distributions and their uncertainties at NNLO and at LO", *Nucl. Phys. B* **855** (2012) 153, doi:10.1016/j.nuclphysb.2011.09.024, arXiv:1107.2652.

[79] NNPDF Collaboration, "Parton distributions with QED corrections", *Nucl. Phys. B* **877** (2013) 290, doi:10.1016/j.nuclphysb.2013.10.010, arXiv:1308.0598.

[80] B. Andersson, G. Gustafson, G. Ingelman, and T. Sjöstrand, "Parton fragmentation and string dynamics", *Phys. Rept.* **97** (1983) 31, doi:10.1016/0370-1573(83)90080-7.

[81] CMS Collaboration, "Event generator tunes obtained from underlying event and multiparton scattering measurements", *Eur. Phys. J. C* **76** (2016) 155, doi:10.1140/epjc/s10052-016-3988-x, arXiv:1512.00815.

[82] G. Corcella et al., "HERWIG 6: an event generator for hadron emission reactions with interfering gluons (including supersymmetric processes)", *JHEP* **01** (2001) 010, doi:10.1088/1126-6708/2001/01/010, arXiv:hep-ph/0011363.

[83] J. Pumplin et al., "New generation of parton distributions with uncertainties from global QCD analysis", *JHEP* **07** (2002) 012, doi:10.1088/1126-6708/2002/07/012, arXiv:hep-ph/0201195.

[84] B. R. Webber, "A QCD model for jet fragmentation including soft gluon interference", *Nucl. Phys. B* **238** (1984) 492, doi:10.1016/0550-3213(84)90333-X.

[85] J. M. Butterworth, J. R. Forshaw, and M. H. Seymour, "Multiparton interactions in photoproduction at HERA", *Z. Phys. C* **72** (1996) 637, doi:10.1007/s002880050286, arXiv:hep-ph/9601371.

[86] GEANT4 Collaboration, "GEANT4—a simulation toolkit", *Nucl. Instrum. Meth. A* **506** (2003) 250, doi:10.1016/S0168-9002(03)01368-8.

[87] D0 Collaboration, "Hard single diffraction in $\overline{\mathrm{p}}\mathrm{p}$ collisions at $\sqrt{s} = 630$ GeV and 1800 GeV", *Phys. Lett. B* **531** (2002) 52, doi:10.1016/S0370-2693(02)01364-3, arXiv:hep-ex/9912061.

[88] CDF Collaboration, "Diffractive dijets with a leading antiproton in $\overline{\mathrm{p}}\mathrm{p}$ collisions at $\sqrt{s} = 1800$ GeV", *Phys. Rev. Lett.* **84** (2000) 5043, doi:10.1103/PhysRevLett.84.5043.

[89] CDF Collaboration, "Diffractive dijet production at $\sqrt{s} = 630$ GeV and 1800 GeV at the Fermilab Tevatron", *Phys. Rev. Lett.* **88** (2002) 151802, doi:10.1103/PhysRevLett.88.151802, arXiv:hep-ex/0109025.

[90] CDF Collaboration, "Observation of exclusive dijet production at the Fermilab Tevatron $\overline{\mathrm{p}}\mathrm{p}$ Collider", *Phys. Rev. D* **77** (2008) 052004, doi:10.1103/PhysRevD.77.052004, arXiv:0712.0604.

[91] CDF Collaboration, "Diffractive Dijet Production in $\overline{\mathrm{p}}\mathrm{p}$ Collisions at $\sqrt{s} = 1.96$ TeV", *Phys. Rev. D* **86** (2012) 032009, doi:10.1103/PhysRevD.86.032009, arXiv:1206.3955.

[92] H1 Collaboration, "Diffractive dijet production with a leading proton in ep collisions at HERA", *JHEP* **05** (2015) 056, doi:10.1007/JHEP05(2015)056, arXiv:1502.01683.

[93] P. Świerska and M. Trzebiński, "BFKL amplitude parametrization for the jet-gap-jet events at the LHC energies", *Acta Phys. Polon. B* **46** (2015) 2477, doi:10.5506/APhysPolB.46.2477, arXiv:1504.06271.

[94] M. Hentschinski, J. D. Madrigal Martínez, B. Murdaca, and A. Sabio Vera, "The next-to-leading order vertex for a forward jet plus a rapidity gap at high energies", *Phys. Lett. B* **735** (2014) 168, doi:10.1016/j.physletb.2014.06.022, arXiv:1404.2937.

[95] M. Hentschinski, J. D. Madrigal Martínez, B. Murdaca, and A. Sabio Vera, "The gluon-induced Mueller-Tang jet impact factor at next-to-leading order", *Nuclear Physics B* **889** (2014) 549, doi:10.1016/j.nuclphysb.2014.10.026, arXiv:1409.6704.

[96] CDF Collaboration, "Dijet production by double pomeron exchange at the Fermilab Tevatron", *Phys. Rev. Lett.* **85** (2000) 4215, doi:10.1103/PhysRevLett.85.4215.